TITLE

Cytokinin receptor AHK3 modulates root-to-shoot transport of *trans*-zeatin-type cytokinin

AUTHORS

Kota Monden[a†], Takamasa Suzuki[b], Mikiko Kojima[c], Yumiko Takebayashi[c], Takehiro Kamiya[d], Takatoshi Kiba[e,f], Hitoshi Sakakibara[c,f], Tsuyoshi Nakagawa[a], and Takushi Hachiya[a]

[a]Department of Molecular and Functional Genomics, Interdisciplinary Center for Science Research, Shimane University, 1060 Nishikawatsu-cho, Matsue, Shimane 690-8504, Japan

[b]College of Bioscience and Biotechnology, Chubu University, 1200 Matsumoto-cho, Kasugai, Aichi 487-8501, Japan

[c]RIKEN Center for Sustainable Resource Science, 1-7-22 Suehiro-cho, Tsurumi-ku, Yokohama, Kanagawa 230-0045, Japan

[d]Graduate School of Agricultural and Life Sciences, Tokyo University, 1-1-1 Yayoi, Bunkyo-ku, Tokyo 113-8657, Japan

[e]Institute of Plant Science and Resources, Okayama University, 2-20-1 Chuo, Kurashiki, Okayama 710-0046, Japan

[f]Graduate School of Bioagricultural Sciences, Nagoya University, Furo-cho, Chikusa-ku, Nagoya, Aichi 464-8601, Japan

[†]Corresponding author: Kota Monden (n23d203@matsu.shimane-u.ac.jp)

AUTHOR STATEMENT

The author responsible for distribution of materials integral to the findings presented in this article in accordance with the policy described in the Instructions for Authors (https://academic.oup.com/plphys/pages/General-Instructions) is Kota Monden.

RUNNING HEAD

AHK3 modulates long-distance cytokinin transport.

ABSTRACT

Trans-zeatin (*t*Z)-type cytokinins are synthesized in roots in response to nitrogen availability, transported to shoot via xylem, and coordinate diverse physiological processes in aerial organs. Within this mechanism, the regulation of cytokinin biosynthesis by nitrate signaling via NIN-like protein 7 as well as the loading of *t*Z-type cytokinins into xylem by ATP-binding cassette transporter G14 have been well studied. However, the roles of other components remain unclear. Here, we show that cytokinin perception and degradation in roots, as mediated by Arabidopsis histidine kinase 3 (AHK3) and cytokinin oxidase/dehydrogenase 4 (CKX4), modulate root-to-shoot transport of *t*Z-type cytokinins. Grafting experiments demonstrated that root-specific *AHK3* deficiency systemically increased leaf blade area through long-distance signals of root-derived *t*Z-type cytokinin, perceived by shoot-expressed AHK3. Transcriptome, hormonome, and reporter analyses revealed that root-specific *AHK3* deficiency reduced *CKX4* expression in roots, elevating *t*Z-type cytokinin levels in roots and xylem sap and thereby enhancing leaf cytokinin response. Transfer experiments manipulating root nitrate levels showed that root-specific *AHK3* deficiency promoted leaf blade area in a manner dependent on both nitrate and root-derived *t*Z-type cytokinin signaling. Moreover, both nitrate signals and root-expressed AHK3 are required for maximal *CKX4* induction in roots, and root-specific *CKX4* deficiency enhanced leaf blade area in a nitrate-dependent manner. These findings reveal a novel mechanism in which an AHK3–CKX4 module governs root-to-shoot transport of *t*Z-type cytokinins, fine-tuning leaf size according to nitrogen availability in roots.

INTRODUCTION

Cytokinins (CKs) are essential plant hormones that coordinate diverse developmental and physiological processes, including cell division, shoot and root growth, vascular formation, and responses to stress and nutrients (Werner et al., 2001; Riefler et al., 2006; Matsumoto-Kitano et al., 2008; Sakakibara, 2021). In *Arabidopsis*, the biologically active CK forms include N^6-(Δ^2-isopentenyl) adenine (iP) and *trans*-zeatin (*t*Z). The initial and rate-limiting step of CK biosynthesis involves N^6-prenylation of adenosine 5′-phosphates catalyzed by adenosine phosphate-isopentenyltransferases (IPTs), producing iP-riboside 5′-phosphates (iPRPs) (Takei et al., 2001a; Miyawaki et al., 2006). These intermediates

are subsequently hydroxylated by cytochrome P450 monooxygenases CYP735A1 and CYP735A2 to form *t*Z-riboside 5′-phosphates (*t*ZRPs) (Takei et al., 2004a). Ribotide precursors are then converted into iP and *t*Z by CK-activating enzyme members of the lonely guy (LOG) family (Kurakawa et al., 2007; Kuroha et al., 2009). CK homeostasis is further modulated by reversible *O*-glucosylation and tentatively reversible *N*-glucosylation catalyzed by glucosyltransferases (UGTs), and by irreversible degradation by cytokinin oxidase/dehydrogenases (CKXs) (Werner et al., 2006; Wang et al., 2011; Jin et al., 2013; Wang et al., 2013; Hošek et al., 2020). CK perception and signaling rely on a multistep His-to-Asp phosphorelay system (Hutchison and Kieber, 2002; Müller and Sheen, 2007). Three membrane-spanning histidine kinases, Arabidopsis histidine kinase (AHK)2, AHK3, and CRE1/AHK4, act as CK receptors (Inoue et al., 2001). Upon ligand binding, the phosphoryl group is transferred from AHKs to histidine phosphotransfer proteins, which shuttle into the nucleus and activate type-B response regulators (Hutchison and Kieber, 2002; Müller and Sheen, 2007). These transcription factors induce CK-responsive genes, including type-A response regulators that function as negative feedback elements (To et al., 2004).

In addition to local roles, CKs act as long-distance signaling molecules that coordinate developmental and physiological processes between roots and shoots (Sakakibara, 2021). In *Arabidopsis*, *t*Z-type CKs predominate in xylem sap, whereas iP-type CKs are more abundant in phloem sap (Hirose et al., 2008; Osugi et al., 2017). This distribution reflects tissue-specific expression of CK biosynthetic genes: *CYP735A2* is strongly expressed in root vasculature, while *IPT3* is mainly expressed in phloem tissues of both roots and shoots (Miyawaki et al., 2004; Takei et al., 2004a,b; Kiba et al., 2013). These activities establish a directional flow of CK species, with root-derived *t*Z-type CKs transported to shoots via xylem and shoot-derived iP-type CKs transported to roots via phloem tissue (Hirose et al., 2008; Matsumoto-Kitano et al., 2008; Kiba et al., 2013). A central component of the root-to-shoot CK transport system is ATP-binding cassette transporter G14 (ABCG14), which loads CKs into xylem in root stele and also contributes to phloem unloading in shoots (Ko et al., 2014; Zhang et al., 2014; Zhao et al., 2021). Heterologous transport assays in yeast have shown that ABCG14 transports multiple CK species, including both iP- and *t*Z-types, underscoring its pivotal role in systemic CK distribution and signaling (Zhao et al., 2023).

97 Root-to-shoot CK transport has been found to be tightly linked to plant
98 nitrogen status. For example, supplying inorganic nitrogen to root activates CK signaling
99 in leaves and increases xylem transport of *t*Z-riboside (*t*ZR) following nitrate application
100 (Sakakibara et al., 1998; Takei et al., 2001b). Moreover, nitrate-induced changes in leaf
101 growth rate correlate with *t*Z and *t*ZR levels in xylem sap and leaves (Rahayu et al., 2005).
102 In *Arabidopsis*, nitrate signaling regulates expression of *IPT3* and *CYP735A2* through
103 NIN-like protein 7 (NLP7) and Nitrate-inducible GARP-type transcriptional repressor 1s
104 (NIGT1s), these transcription factors that are central to the primary nitrate response
105 (Miyawaki et al., 2004; Takei et al., 2004a,b; Kiba et al., 2018; Maeda et al., 2018; Liu
106 et al., 2022). It has been proposed that nitrate signaling mediated by NLP7 coordinates
107 CK metabolism and root-to-shoot CK transport to modulate shoot CK responses (Abualia
108 et al., 2022). In addition, long-distance signals of root-derived *t*Z and *t*ZR differentially
109 affect leaf growth traits, and their ratios in xylem sap are known to be modulated by
110 nitrogen supply (Osugi et al., 2017). Together, these findings highlight that regulation of
111 root-to-shoot CK transport is critical for fine-tuning leaf growth in response to nitrogen
112 availability in roots.
113 Our previous study proposed that root-expressed CK receptors are involved
114 in the regulation of root-to-shoot CK transport. Using grafting, we showed that root-
115 specific deficiencies of *AHK2* and *AHK3* increased iP- and *t*Z-type CK levels in roots by
116 suppressing CK degradation and inducing CK biosynthesis. This rise in root CK content
117 was accompanied by higher *t*Z-type CK levels and stronger expression of CK-inducible
118 genes in shoots (Monden et al., 2022). Notably, among the three CK receptors, *AHK3*
119 was identified as one of the top genes co-expressed with *NLP7* (Supplementary Table S1),
120 suggesting that AHK3 may act in association with nitrate responses via NLP7. In addition,
121 AHK3 has been reported to exhibit a higher affinity for *t*Z than for iP (Stolz et al., 2011),
122 implying a preferential role in *t*Z-type CK signaling. Together, these findings suggest that
123 root-expressed AHK3 may modulate root-to-shoot transport of *t*Z-type CKs in response
124 to nitrogen availability in roots, although the underlying mechanism and physiological
125 relevance remain unclear.
126 In this study, we show that CK perception and degradation in roots, mediated
127 by AHK3 and CKX4, modulate root-to-shoot transport of *t*Z-type CKs. Growth analyses
128 of grafted plants demonstrated that root-specific *AHK3* deficiency enlarged leaf blade

129 area through long-distance signals of root-derived *t*Z-type CK, perceived by shoot-
130 expressed AHK3. Transcriptome, hormonome, and reporter assays further revealed that
131 root-specific *AHK3* deficiency reduced *CKX4* expression in roots, elevating *t*Z-type CK
132 levels in roots and xylem sap and thereby enhancing CK responses in leaves. Transfer
133 experiments manipulating root nitrate levels showed that nitrate-induced leaf growth
134 promotion depends on long-distance signals of root-derived *t*Z-type CK, which is in turn
135 controlled by root-expressed AHK3 and CKX4. We propose a mechanism in which the
136 AHK3–CKX4 module governs root-to-shoot transport of *t*Z-type CK in response to
137 nitrogen availability in roots, thereby fine-tuning leaf size to maintain balanced plant
138 growth.
139
140 **RESULTS**
141 **1. Root-expressed AHK3 modulates shoot and root growth**
142 To identify which root-expressed CK receptor(s) influence shoot and root growth, we
143 grafted Col-0 (WT) scions onto rootstocks derived from WT, single mutant (i.e., *ahk2-5*;
144 *ahk2*, *ahk3-7*; *ahk3*, *cre1-2*; *ahk4*) or double mutant (i.e., *ahk2-5 ahk3-7*; *ahk23*, *ahk2-5*
145 *cre1-2*; *ahk24*, *ahk3-7 cre1-2*; *ahk34*) five-day-old seedlings (Riefler et al., 2006).
146 Five days after grafting, we selected plants (scion/rootstock: WT/WT, WT/*ahk2*,
147 WT/*ahk3*, WT/*ahk4*, WT/*ahk23*, WT/*ahk24*, WT/*ahk34*) for further analysis if they
148 showed vigorous growth without adventitious roots. Grafted plants were then cultivated
149 for 7 days on either half-strength MS (1/2 MS) medium or nutrient-rich soil. We measured
150 shoot fresh weight, leaf blade area, and leaf number. Overall, WT/*ahk3*, WT/*ahk23*, and
151 WT/*ahk34* displayed greater shoot growth than WT/WT (Fig. 1A, Supplementary Fig.
152 S1A). Relative to the WT/WT control, these lines showed an increase in shoot fresh
153 weight of 26%, 35%, and 19%, and in leaf blade area of 26%, 32%, and 17%, respectively
154 (Fig. 1, B and C). Under nutrient-rich soil conditions, shoot fresh weight increased by
155 34%, 25%, and 22%, and leaf blade area by 32%, 21%, and 17% in WT/*ahk3*, WT/*ahk23*,
156 and WT/*ahk34*, respectively, compared with WT/WT (Supplementary Fig. S1, B and C).
157 Leaf number was generally similar across grafted plants in both conditions, although
158 several statistically significant differences were noted (Fig. 1D, Supplementary Fig. S1D).
159 We next monitored primary root length in grafted plants transferred to 1/2 MS medium
160 over a five-day period. Primary root length was comparable at day 0, but WT/*ahk3*,

161 WT/*ahk23*, and WT/*ahk34* developed significantly shorter roots than WT/WT from day
162 3 onward (Supplementary Fig. S2). In contrast, WT/*ahk2*, WT/*ahk4*, and WT/*ahk24*
163 showed no significant differences in shoot or root growth relative to WT/WT (Fig. 1,
164 Supplementary Figs. S1 and S2). Notably, the relative growth of WT/*ahk3* was
165 comparable to WT/*ahk23* and WT/*ahk34*, indicating that loss of AHK3 alone is sufficient
166 to alter overall plant growth. We therefore focused subsequent analyses on WT/*ahk3*,
167 using WT/WT, WT/*ahk2*, and WT/*ahk4* as comparisons.
168
169 **2. Root-expressed AHK3 modulates root CK levels**
170 Our previous work showed that root-specific deficiencies of *AHK2* and *AHK3* markedly
171 increased iP- and *t*Z-type CK levels in roots, but the receptor responsible for governing
172 root CK levels was unclear (Monden et al., 2022). To clarify this, we measured iP- and
173 *t*Z-type CK concentrations in WT/WT, WT/*ahk2*, WT/*ahk3*, and WT/*ahk4* roots. Root
174 concentrations of both iP- and *t*Z-type CKs were significantly elevated in WT/*ahk3*
175 compared with WT/WT; moreover, this was true for active, precursor, and inactive forms
176 (Fig. 2, Supplementary Fig. S3). In contrast, root iP- and *t*Z-type CKs were largely
177 unchanged in WT/*ahk2* and WT/*ahk4* relative to WT/WT, except for iP7G and iP9G in
178 WT/*ahk4* (Fig. 2, Supplementary Fig. S3). These findings indicate that AHK3 expressed
179 in roots modulates CK homeostasis.
180
181 **3. Root-expressed AHK3 influences the root transcriptome**
182 Despite the fact that *AHK2*, *AHK3*, and *AHK4* are all expressed in roots (Higuchi et al.,
183 2004), only AHK3 strongly affected root CK levels. This suggests that each CK receptor
184 may regulate a distinct set of downstream genes. To test this hypothesis, we performed
185 an RNA-seq analysis of root samples taken from WT/WT, WT/*ahk2*, WT/*ahk3*, and
186 WT/*ahk4*. All data, including raw read counts, reads per million mapped reads (RPM),
187 and normalized transcript levels are presented in Supplementary Tables S2–4. First, we
188 examined differentially expressed genes (DEGs) between the roots of the WT/WT control
189 and three grafted plants, i.e., WT/*ahk2*, WT/*ahk3*, and WT/*ahk4* (Supplementary Table
190 S6). An analysis of the DEGs with a fold change of 1.5 or greater revealed that 62 genes
191 were significantly upregulated in WT/*ahk3* relative to WT/WT roots, whereas 91 genes
192 were downregulated (Fig. 3A, Supplementary Figs. S4 and S5). Notably, relatively few

193 DEGs were detectable in the roots of WT/*ahk2* and WT/*ahk4* (Fig. 3A, Supplementary
194 Figs. S4 and S5). Next, we conducted a Gene Ontology (GO) term enrichment analysis
195 of the 62 upregulated genes and the 87 downregulated genes (excluding *AHK3*) identified
196 in WT/*ahk3* roots. This revealed that multiple hormone-related terms were enriched in
197 both sets (Supplementary Fig. S6). To further examine the extent to which CK receptor
198 regulates CK signaling-related genes in roots, we analyzed the expression of CK-
199 inducible and -repressible genes in the roots of grafted plants; to do so we used a curated
200 gene list (Bhargava et al., 2013). We found that the expression levels of both CK-
201 inducible and -repressible genes in the roots of WT/*ahk4* were comparable to the levels
202 detected in WT/WT (Fig. 3B). In contrast, the expression of CK-inducible genes in root
203 tissue samples was significantly lower in both WT/*ahk2* and WT/*ahk3* relative to the
204 WT/WT (Fig. 3B). Moreover, CK-repressible genes were significantly increased in
205 WT/*ahk3* and showed an increasing trend in WT/*ahk2* (Fig. 3B). Notably, the magnitude
206 of these changes was more pronounced in WT/*ahk3* than in WT/*ahk2* roots, suggesting
207 that root-expressed AHK3 plays a major role in regulating root CK signaling.
208 Next, to identify candidate gene(s) that may be responsible for increased CK
209 levels in WT/*ahk3* roots, we examined whether the DEGs observed in WT/*ahk3* roots
210 included genes that are known to be involved in CK biosynthesis and inactivation. Of
211 these genes, only *CKX4*, which is involved in CK degradation, was among the genes that
212 were downregulated genes in WT/*ahk3* roots relative to the WT/WT (Fig. 3, A and C).
213 Quantitative RT-PCR (qRT-PCR) analysis confirmed that expression of *CKX4* in roots
214 was significantly decreased in WT/*ahk3* relative to WT/WT (Fig. 3D). Taken together,
215 these results suggest that root-expressed AHK3 modulates root CK levels, potentially via
216 CKX4-mediated CK degradation.
217
218 **4. Root-expressed AHK3 modulates *t*Z-type CKs in xylem sap**
219 CKs synthesized in roots are transported to shoots mainly via xylem pathway (Ko et al.,
220 2014; Osugi et al., 2017). Given that we observed relatively high CK levels in WT/*ahk3*
221 roots, we hypothesized that the CK levels of xylem sap may also be altered. To verify
222 this, we measured the CK concentrations of xylem sap samples from WT/WT, WT/*ahk2*,
223 WT/*ahk3*, and WT/*ahk4*. We found that *t*Z, *t*ZR, and *t*ZRPs were relatively more
224 abundant than inactive forms of *t*Z-type CK and iP-type CKs in WT/WT xylem sap

225 (Supplementary Fig. S7A). This suggests that there is preferential root-to-shoot transport
226 of *t*Z and its precursors. Notably, the concentrations of *t*Z-type CKs were significantly
227 higher in WT/*ahk3* than in WT/WT xylem sap, while the concentrations of iP-type CKs
228 remained largely unchanged (Fig. 4, Supplementary Fig. S7B). Among the major CK
229 species detected in xylem sap, the concentration of *t*Z showed a 2.22-fold increase in
230 WT/*ahk3* relative to WT/WT xylem sap (Fig. 4B). In contrast, the concentrations of *t*ZR
231 and *t*ZRPs were both slightly higher in WT/*ahk3* than in WT/WT xylem sap, showing
232 1.20-fold and 1.37-fold increases, respectively (Fig. 4B). Finally, the concentrations of
233 iP- and *t*Z-type CKs were largely unchanged in WT/*ahk2* and WT/*ahk4* relative to
234 WT/WT xylem sap, except for *t*Z and *t*ZRPs in WT/*ahk4* (Fig. 4, Supplementary Fig.
235 S7B). Overall, these results suggest that root-expressed AHK3 modulates the root-to-
236 shoot transport of *t*Z-type CKs, especially *t*Z.
237
238 **5. Root-expressed AHK3 systemically influences the shoot transcriptome**
239 Next, to test whether elevated *t*Z-type CK levels in WT/*ahk3* xylem sap affected shoot
240 CK levels, we measured CK concentrations in WT/WT, WT/*ahk2*, WT/*ahk3*, and
241 WT/*ahk4* shoots. Unexpectedly, *t*Z-type CK concentrations were not higher in WT/*ahk3*
242 than in WT/WT shoots, except for *t*Z9G (Supplementary Fig. S8). Similarly, almost all
243 CK species in WT/*ahk2* and WT/*ahk4* showed no marked differences compared with
244 WT/WT (Supplementary Fig. S8). We next analyzed whether root-specific CK receptor
245 deficiency may alter the shoot transcriptomes. To do so, we performed RNA-seq on
246 WT/WT, WT/*ahk2*, WT/*ahk3*, and WT/*ahk4* shoots. Raw read counts, RPM, and
247 normalized transcript levels are provided in Supplementary Tables S2, S3, and S5.
248 Differential expression analysis with a 1.5-fold cutoff revealed 163 genes significantly
249 upregulated and 35 genes downregulated in WT/*ahk3* relative to WT/WT shoots (Fig. 5A,
250 Supplementary Table S7). No DEGs were detected in WT/*ahk2* or WT/*ahk4* shoots (Fig.
251 5A, Supplementary Table S7). Moreover, the number of upregulated genes was about
252 five times greater than the number of downregulated genes in WT/*ahk3* shoots (Fig. 5A,
253 Supplementary Table S7). This finding indicates that root-specific *AHK3* deficiency
254 mainly induces gene expression in shoots.
255 To gain insight into the functional characteristics of the upregulated set, we
256 performed GO enrichment analysis using the set of 163 upregulated genes. Enriched

257 categories included "Translation," "Response to inorganic substance," and "Cellular
258 nitrogen compound biosynthetic process" (Fig. 5B), indicating activation of genes related
259 to protein synthesis, nutrient responses, and nitrogen metabolism in WT/*ahk3* shoots. We
260 then examined whether these transcriptional changes correlated with altered shoot
261 element concentrations. We found that the shoot concentrations of calcium, sulfur,
262 manganese, and molybdenum were significantly higher in WT/*ahk3* than in WT/WT
263 (Supplementary Fig. S9), suggesting a possible association between these nutrients and
264 altered gene expression in WT/*ahk3* shoots. In contrast, although several nitrogen-related
265 GO terms were enriched, shoot concentrations of nitrogen and nitrate did not differ
266 between WT/WT and WT/*ahk3* (Supplementary Fig. S9). Thus, nitrogen status in
267 WT/*ahk3* shoots did not drive the transcriptional changes observed in protein synthesis
268 and nitrogen metabolism genes. Because nitrogen is a major protein component and both
269 nitrate and CK signaling promote expressions of protein synthesis-related genes
270 (Sakakibara et al., 2006), altered CK response in WT/*ahk3* shoots may underlie these
271 transcriptional effects.
272 To further assess CK response, we compared the 163 upregulated genes in
273 WT/*ahk3* shoots with CK-inducible genes (Bhargava et al., 2013). *Arabidopsis response*
274 *regulator 5* (*ARR5*) and *Glutaredoxin-S6* (*GrxS6*) were among the overlapping genes (Fig.
275 5A). *ARR5*, one of ten type-A *ARRs*, is a representative CK-responsive gene functioning
276 as a negative feedback regulator of CK signaling (To et al., 2004). Expression of several
277 other type-A *ARRs* also tended to increase in WT/*ahk3* relative to WT/WT (Fig. 5C).
278 Consistent with the RNA-seq results, qRT-PCR confirmed that *ARR5* expression was
279 significantly higher in WT/*ahk3* shoots than in WT/WT (Fig. 5D). Taken together, these
280 results indicate that root-expressed AHK3 modulates shoot gene expression, at least
281 partly through CK signaling.
282
283 **6. Root-derived CK signals are required for enhanced shoot growth via root-**
284 **expressed AHK3**
285 Elevated *t*Z-type CKs in WT/*ahk3* xylem sap suggested that long-distance signals of root-
286 derived *t*Z-type CK contribute to enhanced shoot growth. To test this, we generated *ahk3*
287 *abcg14* and *ahk3 cyp735a1 cyp735a2* (*ahk3 cypDM*) mutants by traditional crossing
288 (Supplementary Fig. S10A). Since both *abcg14* and *cypDM* shoots display lack proper

289 root-derived *t*Z-type CK signaling (Kiba et al., 2013; Ko et al., 2014), these mutants allow
290 assessment of its contribution. Disruption of the respective genes in *ahk3 abcg14* and
291 *ahk3 cypDM* was confirmed by RT-PCR (Supplementary Fig. S10B). Grafted plants
292 (scion/rootstock: WT/WT, WT/*ahk3*, WT/*abcg14*, WT/*ahk3 abcg14*, WT/*cypDM*,
293 WT/*ahk3 cypDM*) were cultivated on 1/2 MS medium, and shoot growth was measured.
294 Shoot fresh weight and leaf blade area were significantly reduced in WT/*abcg14* and
295 WT/*ahk3 abcg14*, while WT/*cypDM* and WT/*ahk3 cypDM* showed no decrease
296 compared with WT/WT (Fig. 6, A and B). These results agree with previous findings that
297 root-specific deficiency of *ABCG14* impairs shoot growth, whereas deficiencies of
298 *CYP735A1* and *CYP735A2* do not (Kiba et al., 2013; Ko et al., 2014). Notably, the
299 increases in shoot fresh weight and leaf blade area seen in WT/*ahk3* compared with
300 WT/WT were largely suppressed by disrupting *ABCG14* and completely abolished by
301 disrupting *CYP735A1* and *CYP735A2* in roots (Fig. 6, A and B). These findings indicate
302 that long-distance signals of root-derived *t*Z-type CKs are required for enhanced shoot
303 growth in WT/*ahk3*.
304 To determine which CK receptor(s) mediate CK signaling underlying this
305 growth effect, we analyzed grafted plants carrying single or double mutations in *AHK2*,
306 *AHK3*, or *AHK4* specifically in WT/*ahk3* shoots. Grafted plants (scion/rootstock:
307 WT/WT, WT/*ahk3*, *ahk2*/*ahk3*, *ahk3*/*ahk3*, *ahk4*/*ahk3*, *ahk23*/*ahk3*, *ahk24*/*ahk3*,
308 *ahk34*/*ahk3*) were cultivated under 1/2 MS medium, and shoot growth was measured.
309 Increases in shoot fresh weight and leaf blade area observed in WT/*ahk3* relative to
310 WT/WT were similarly evident in *ahk2*/*ahk3*, *ahk4*/*ahk3*, and *ahk24*/*ahk3* (Fig. 6, C and
311 D). In contrast, these enhancements were suppressed in *ahk3*/*ahk3* and *ahk34*/*ahk3*, and
312 markedly reduced in *ahk23*/*ahk3*, where values were significantly lower than WT/WT
313 (Fig. 6, C and D). These results indicate that enhanced shoot growth in WT/*ahk3* depends
314 primarily on CK signaling through shoot-expressed AHK3, with partial contribution from
315 AHK2. Next, to visualize sites of enhanced CK response in WT/*ahk3* shoots, we
316 introduced the synthetic CK reporter *TCSn:GFP* into WT/WT and WT/*ahk3* shoots
317 (Zürcher et al., 2013). Grafted plants (scion/rootstock: *TCSn:GFP*/WT, *TCSn:GFP*/*ahk3*)
318 were grown on 1/2 MS medium. *TCSn:GFP*/*ahk3* exhibited greater shoot fresh weight
319 and leaf blade area than *TCSn:GFP*/WT (Fig. 6E). Notably, GFP fluorescence intensity
320 in true leaf was also significantly higher in *TCSn:GFP*/*ahk3* than in *TCSn:GFP*/WT (Fig.

321 6F). Finally, to examine how root-specific *AHK3* deficiency influences leaf micro-
322 morphology, we measured epidermal cell size and number in true leaves of WT/WT and
323 WT/*ahk3*. Cell size was comparable between genotypes, but cell number was
324 significantly higher in WT/*ahk3* than in WT/WT (Fig. 6G). These results suggest that
325 root-specific *AHK3* deficiency enhances leaf CK response, promoting epidermal cell
326 division and thereby increasing leaf size.
327
328 **7. Root-expressed AHK3 modulates leaf size in a nitrate-dependent manner**
329 *AHK3* was identified as one of the top genes co-expressed with the nitrate sensor NLP7
330 (Supplementary Table S1), suggesting that AHK3 may play a role in plant nitrate
331 responses. To test this, we manipulated the nitrate levels of WT/WT and WT/*ahk3* roots.
332 Ten-day-old WT/WT and WT/*ahk3* were first transferred to 2.5 mM ammonium
333 succinate (5 mM NH_4^+) medium and incubated for 48 hours to deplete nitrate
334 (Supplementary Fig. S11A). Grafted plants were then transferred to medium containing
335 5 mM NH_4^+ supplemented with either 0.5 mM KNO_3 (KNO_3) or 0.5 mM KCl (KCl) and
336 grown for 5 days to assess the presence or absence of nitrate signaling in roots. Nitrate
337 accumulated only in WT/WT and WT/*ahk3* roots grown under KNO_3 (Supplementary
338 Fig. S11B). Moreover, WT/WT and WT/*ahk3* appeared healthy, with comparable shoot
339 chlorophyll concentrations under both conditions (Supplementary Fig. S12), indicating
340 that nitrogen deficiency or ammonium toxicity did not occur. In WT/WT, shoot fresh
341 weight and leaf blade area were found to be significantly greater under KNO_3 than KCl
342 (Fig. 7A), showing that nitrate signaling promotes leaf growth. Notably, shoot fresh
343 weight and leaf blade area were similar between WT/WT and WT/*ahk3* under KCl, but
344 were significantly higher in WT/*ahk3* than in WT/WT under KNO_3 (Fig. 7A).
345 Next, to test whether nitrate-dependent growth promotion in WT/*ahk3*
346 requires root-derived *t*Z-type CK signals, we analyzed WT/*abcg14* and WT/*ahk3 abcg14*
347 grown under KNO_3 or KCl. Interestingly, the increases in shoot fresh weight and leaf
348 blade area observed in WT/WT and WT/*ahk3* under KNO_3 were strongly suppressed in
349 WT/*abcg14* and WT/*ahk3 abcg14* (Fig. 7B). These results indicate that long-distance
350 signals of root-derived *t*Z-type CKs are required for nitrate-induced leaf growth
351 promotion. Moreover, shoot fresh weight and leaf blade area were comparable between

352 WT/*abcg14* and WT/*ahk3 abcg14* under KNO_3 (Fig. 7B), suggesting that root-derived
353 *t*Z-type CK signals may contribute to the enhanced leaf growth of WT/*ahk3*.
354 To further clarify the role of AHK3 in nitrate signaling, we analyzed
355 expression of CK biosynthesis and inactivation genes in roots 4 hours after transfer to
356 KNO_3 or KCl. Nitrate accumulation was detected only in WT/WT and WT/*ahk3* roots
357 after KNO_3 treatment (Supplementary Fig. S11C). In WT/WT, root expression of *IPT3*,
358 *CYP735A1*, *CYP735A2*, and *CKX4* was significantly higher under KNO_3 than KCl (Fig.
359 7C, Supplementary Fig. S13), indicating induction by nitrate signaling. Importantly,
360 expression of *IPT3*, *CYP735A1*, and *CYP735A2* was similar in WT/WT and WT/*ahk3*
361 under KNO_3, whereas *CKX4* expression was significantly reduced in WT/*ahk3* compared
362 with WT/WT (Fig. 7C, Supplementary Fig. S13). These results suggest that both nitrate
363 signals and root-expressed AHK3 are required for maximal *CKX4* induction.
364 To investigate the role of CKX4 in nitrate signaling, we obtained two
365 independent T-DNA alleles, *ckx4-1* (SALK_055204) and *ckx4-2* (SALK_132516), from
366 the Arabidopsis Biological Resource Center. *Ckx4-1* carries an intron insertion (Bartrina
367 et al., 2011), while *ckx4-2* carries an exon insertion (Supplementary Fig. S14). RT-PCR
368 confirmed reduced *CKX4* transcript in *ckx4-1* and absence in *ckx4-2* (Fig. 7D), indicating
369 that *ckx4-1* is a knockdown and *ckx4-2* a knockout. Grafted plants (scion/rootstock:
370 WT/WT, WT/*ckx4-1*, WT/*ckx4-2*) were cultivated under KNO_3 or KCl, and shoot growth
371 was measured. Under KCl, shoot fresh weight and leaf blade area were similar among
372 genotypes (Fig. 7E). Under KNO_3, however, both traits were significantly greater in
373 WT/*ckx4-1* and WT/*ckx4-2* compared to WT/WT (Fig. 7E).
374 To further clarify relationship between AHK3 and CKX4, we generated *ahk3*
375 *ckx4-1* and *ahk3 ckx4-2* mutants by traditional crossing (Supplementary Fig. S15, A and
376 B). Grafted plants (scion/rootstock: WT/WT, WT/*ahk3*, WT/*ckx4-1*, WT/*ckx4-2*,
377 WT/*ahk3 ckx4-1*, WT/*ahk3 ckx4-2*) were grown under KNO_3 or KCl, and shoot growth
378 was measured. All genotypes showed comparable shoot growth under KCl
379 (Supplementary Fig. S15C). Under KNO_3, however, shoot fresh weight and leaf blade
380 area were significantly greater in WT/*ahk3*, WT/*ckx4-1*, WT/*ckx4-2*, WT/*ahk3 ckx4-1*,
381 and WT/*ahk3 ckx4-2* compared with WT/WT (Supplementary Fig. S15C). These traits
382 were higher in WT/*ahk3* than in WT/*ckx4-1* and WT/*ckx4-2* (Supplementary Fig. S15C),
383 indicating that CKX4 acts downstream of AHK3. Importantly, WT/*ahk3 ckx4-1* and

384 WT/*ahk3 ckx4-2* showed no further growth increase relative to WT/*ahk3* under KNO_3
385 (Supplementary Fig. S15C). Together, these results suggest that nitrate-induced leaf
386 growth promotion occurs through a pathway mediated jointly by AHK3 and CKX4.
387
388 **DISCUSSION**
389 Recent studies have shown that long-distance signals of root-derived *t*Z-type CK
390 coordinate multiple physiological processes in aerial organs, including leaf growth,
391 photoperiod stress response, shade avoidance, and flowering time (Osugi et al., 2017;
392 Landrein et al., 2018; Frank et al., 2020; Gautrat et al., 2024; Bartrina et al., 2025). These
393 findings highlight that proper regulation of root-to-shoot *t*Z-type CK transport is essential
394 for plants to adapt to environmental fluctuations.
395 Based on our findings and prior studies (Miyawaki et al., 2004; Kiba et al.,
396 2013; Ko et al., 2014; Zhang et al., 2014; Sakakibara, 2021, 2025), we provide new
397 insight into the specific mechanisms responsible for modulating root-to-shoot *t*Z-type CK
398 transport, as mediated by CK perception and degradation through an AHK3–CKX4
399 module. Nitrate signaling promotes *t*Z-type CK biosynthesis in pericycle and phloem
400 companion cells via IPT3, CYP735A2, and related enzymes. *t*Z-type CKs are then
401 transported to the extracellular and endoplasmic reticulum (ER) space by transporters
402 such as ABCG14. Active form *t*Z are perceived by AHK3 on plasma membrane (PM)
403 and ER membrane. Activation of CK signaling through AHK3 induces expression of
404 *CKX4*, predicted to localize in apoplast, where it modulates apoplastic *t*Z-type CK levels
405 by degradation. These mechanisms likely influence the apoplastic *t*Z-type CK pool and,
406 consequently, the amount of *t*Z-type CK loaded into xylem (Supplementary Fig. S16). To
407 further substantiate this model, it will likely be necessary to analyze the spatial expression
408 patterns of AHK3 and CKX4 at the tissue and cellular level in future studies. Interestingly,
409 *IPT3* expression and *t*Z-type CK levels in roots also respond to other nutrients, including
410 phosphate, sulfate, and potassium (Hirose et al., 2008; Nam et al., 2012). Thus, AHK3
411 may modulates *t*Z-type CK levels in response to diverse nutrient signals. Collectively,
412 the AHK3–CKX4 module could serve as a feedback regulator that attenuates the nutrient-
413 induced root-to-shoot transport of *t*Z-type CKs, thereby fine-tuning leaf CK response to
414 maintain balanced plant growth.

415 CKXs are known to mediate irreversible CK degradation, producing adenine
416 (or its derivatives) and aldehyde (Schmülling et al., 2003). In *Arabidopsis*, seven CKXs
417 differ in substrate specificity, spatial and temporal expression, and subcellular
418 localization, targeting either vacuoles (CKX1, CKX3), ER (CKX1), apoplasts (CKX2,
419 CKX4, CKX5, CKX6), or the cytosol (CKX7) (Werner et al., 2003; Galuszka et al., 2007;
420 Frébort et al., 2011; Niemann et al., 2018). Expression of *CKX3*, *CKX4*, *CKX5*, and *CKX6*
421 is strongly induced by CK treatment (Werner et al., 2006), suggesting sensitivity to
422 internal CK levels and roles in maintaining homeostasis. Moreover, CKX2 and CKX4
423 show higher *in vitro* CKX activity than other CKXs, preferentially degrading active form
424 CKs at neutral or slightly basic pH (Galuszka et al., 2007). Our data showed that root-
425 specific *AHK3* deficiency greatly reduced *CKX4* expression in roots, without significantly
426 altering other *CKX*s (Figs. 3 and 7). These findings suggest that root-expressed AHK3
427 modulates *t*Z degradation by inducing *CKX4* expression in response to the internal *t*Z
428 level. This interpretation is supported by our observation that *t*Z concentration was
429 markedly higher in WT/*ahk3* xylem sap than in WT/WT (Fig. 4). Furthermore, Osugi *et*
430 *al.* (2017) demonstrated that root-derived *t*ZR controls both leaf number and area,
431 whereas root-derived *t*Z regulates only leaf area. In WT/*ahk3*, the increase in xylem sap
432 *t*Z relative to WT/WT was greater than that of *t*ZR (Fig. 4). Thus, the enlarged leaf blade
433 area in WT/*ahk3*, without a change in leaf number, likely reflects long-distance signaling
434 by root-derived *t*Z (Figs. 1 and 4).
435 AHK2, AHK3, and AHK4 localize to the PM and ER membrane, where they
436 play central roles in CK signal transduction (Antoniadi et al., 2020; Kubiasová et al.,
437 2020). AHK3 is considered to be primarily localized on the ER membrane and partially
438 on the PM (Caesar et al., 2011; Wulfetange et al., 2011). Therefore, ER-localized AHK3
439 may contribute substantially to regulation of root-to-shoot transport of *t*Z-type CKs.
440 AHK3 is also expressed more strongly in leaves than in roots, and its leaf expression
441 exceeds that of AHK2 and AHK4, supporting its hypothesized role as a major regulator
442 of leaf CK response (Higuchi et al., 2004). This hypothesis is consistent with our finding
443 that leaf growth promotion, driven by increased shoot CK response, was diminished when
444 AHK3 was specifically disrupted in WT/*ahk3* shoots (Fig. 6). Strikingly, root-expressed
445 AHK3 exerted a stronger impact on the root transcriptome and on CK levels than root-
446 expressed AHK2 and AHK4 (Figs. 2 and 3). Taken together, these results suggest that

447 AHK3 also plays a major role in roots. Previous reports indicate that rosette leaf growth,
448 CK metabolism, leaf senescence, and stomatal opening depend particularly on AHK3, as
449 disruption of AHK3, but not other CK receptors, impairs these processes (Riefler et al.,
450 2006; Kim et al., 2006; Arnaud et al., 2017). The distinct functions of these receptors may
451 arise from their expression patterns, recognition of different CK species, and specific
452 interactions with other proteins (Higuchi et al., 2004; Spíchal et al., 2004; Romanov et
453 al., 2006; Stolz et al., 2011). A key feature of AHK3 is its ligand preference: while AHK2
454 and AHK4 bind iP and *t*Z with similar affinity, AHK3 shows higher affinity for *t*Z than
455 iP (Stolz et al., 2011). In addition, AHK3 specifically mediates CK-triggered
456 phosphorylation of ARR2 (Kim et al., 2006). These differences in ligand preference and
457 downstream targets may underlie the unique functions of AHK3.
458 Overall, this study uncovered a comprehensive mechanism by which the CK
459 receptor AHK3 systemically modulates the shoot growth via exerting control of root-to-
460 shoot *t*Z-type CK transport. Furthermore, we clarified the role of AHK3 in modulating
461 leaf size in response to root nitrogen availability, a key environmental factor. Overall,
462 these findings provide new insight into how plants integrate nutritional cues to coordinate
463 systemic communication between roots and shoots.
464

465 **MATERIALS AND METHODS**

466 **Plant materials**

467 The *Arabidopsis thaliana* accession Col-0 was used as wild type. T-DNA insertion lines
468 *ahk2-5*, *ahk3-7*, *cre1-2*, *ahk2-5 ahk3-7*, *ahk2-5 cre1-2*, *ahk3-7 cre1-2* (Riefler et al., 2006),
469 *abcg14* (Ko et al., 2014), *cyp735a1-2 cyp735a2-2* (Kiba et al., 2013), and *ckx4-1*
470 (Bartrina et al., 2011) have been described previously. The *ckx4-2* (SALK_132516) line
471 was obtained from the Arabidopsis Biological Resource Center (https://abrc.osu.edu/).
472 The transgenic line *TCSn:GFP* (Zürcher et al., 2013) was described previously. Finally,
473 the homozygous multiple mutants *ahk3-7 abcg14*, *ahk3-7 cyp735a1-2 cyp735a2-2*, *ahk3-*
474 *7 ckx4-1*, and *ahk3-7 ckx4-2* were generated by crossing, and genotypes were determined
475 by genomic PCR using primers listed in Supplementary Table S8.
476

477 **Growth conditions of grafted plants**

478 Seeds were surface-sterilized and kept in the dark at 4°C for 3 days to break dormancy.
479 Approximately 120 seeds per dish were sown in rectangular dishes (140 × 100 × 20 mm^3;
480 Eiken Chemical Co. Ltd., Tokyo, Japan) containing 50 mL of half-strength MS salts
481 including vitamins (Code: M0222; Duchefa Biochemie), supplemented with 0.05% (w/v)
482 MES-KOH (pH 5.7), 1% (w/v) sucrose, and 0.5% (w/v) gellan gum (Fujifilm Wako, VA,
483 USA). Plants were grown under a 16/8-h light/dark cycle at 22°C with a photosynthetic
484 photon flux density (PPFD) of 25 μmol m^{-2} s^{-1}. Five-day-old seedlings were cut
485 perpendicularly at the hypocotyl using an injection needle tip (Code: NN-2613S;
486 TERUMO, Tokyo, Japan). Excised scions were connected to corresponding rootstocks
487 using silicone microtubes (inner × outer diameter: φ0.4 × φ0.5 mm; Code: 1-8194-04; AS
488 ONE, Osaka, Japan). Grafted plants were incubated for 5 days under continuous light at
489 27°C with a PPFD of 50 μmol m^{-2} s^{-1}. Successfully grafted plants without adventitious
490 roots were selected, transferred to solid media or soil pots, then grown for further
491 experiments.
492 For *in vitro* cultures, grafted plants were grown vertically for five days or
493 horizontally for seven days under a PPFD of 70 μmol m^{-2} s^{-1} (16/8-h light/dark cycle) at
494 22°C in 50 mL (vertical) or 30 mL (horizontal) of half-strength MS salts without vitamins
495 (Code: M0221; Duchefa Biochemie), supplemented with 0.05% (w/v) MES-KOH (pH
496 5.7), 1% (w/v) sucrose, and 0.8% (w/v) purified agar (Code: 01162-15; Nacalai Tesque,
497 Kyoto, Japan). To facilitate non-destructive root sampling during horizontal growth,
498 media surfaces were covered with cellophane sheets (Hachiya et al., 2021).
499 For soil cultivation, grafted plants were grown for 7 days under a PPFD of
500 70 μmol m^{-2} s^{-1} (16/8-h light/dark cycle) at 22°C in pots containing ~150 mL of nutrient-
501 rich soil (Supermix A; Sakata Seed, Kyoto, Japan).
502 For transfer experiments with varying nitrogen concentrations, grafted plants
503 were placed on cellophane sheets in round dishes (diameter 90 mm; depth 20 mm; AS
504 ONE) containing 30 mL of half-strength MS modified basal salt mixture without nitrogen
505 (M531; PhytoTech Labs, Lenexa, KS, USA), supplemented with 2.5 mM $(NH_4)_2C_4H_4O_4$,
506 0.05% (w/v) MES-KOH (pH 5.7), 1% (w/v) sucrose, and 0.8% (w/v) purified agar (Code:
507 01162-15; Nacalai Tesque) (5 mM NH_4^+ medium). Plants were grown for 48 hours under
508 a PPFD of 70 μmol m^{-2} s^{-1} (16/8-h light/dark cycle) at 22°C, then transferred to 5 mM

509 NH_4^+ medium supplemented with either 0.5 mM KNO_3 or 0.5 mM KCl and grown for
510 five days under the same conditions.
511
512 **Growth analysis of grafted plants**
513 Shoots were weighed on a precision balance (HR-202i; A&D, Tokyo, Japan). Leaf blades
514 were harvested and scanned at 600 dpi (GT-X980; EPSON, Tokyo, Japan) to measure
515 true leaf blade area. Roots of vertically grown plants were scanned at 600 dpi to measure
516 primary root length. To monitor root elongation, root tip positions were marked every 24
517 hours. Leaf blade area and primary root length were quantified using ImageJ version 1.53t
518 (US National Institutes of Health, Bethesda, MD, USA).
519
520 **Xylem sap collection**
521 Grafted plants were cut perpendicularly at the hypocotyl using an injection needle tip
522 (Code: NN-2613S; TERUMO). A silicone microtube (inner × outer diameter: φ0.5 × φ0.6
523 mm; Code: 1-8194-05; AS ONE) was attached to the cut end, and plants were incubated
524 for 2 hours to allow exudation. After incubation, the silicone microtube was detached,
525 and xylem sap collected in the tube was recovered by centrifugation into a collection tube.
526 This was then and stored at –80°C until further analysis. We used 12 µL aliquots of sap
527 from each grafted plant for CK analyses.
528
529 **Determination of CK species**
530 CK extraction and quantification followed the method of Kojima *et al*. (2009), using an
531 ultra-performance liquid chromatography–tandem quadrupole mass spectrometry system
532 (AQUITY UPLC System/XEVO-TQS; Waters Corp., Milford, MA, USA) equipped with
533 an octadecylsilyl column (ACQUITY UPLC HSS T3, 1.8 µm, 2.1 mm × 100 mm; Waters
534 Corp.).
535
536 **Extraction of total RNA**
537 To extract total RNA, frozen plant samples were first homogenized using a Multi-Beads
538 Shocker and 5 mm zirconia beads. Total RNA was then isolated with the RNeasy Plant
539 Mini Kit (Qiagen, Hilden, Germany) with all protocols performed as per the

540 manufacturer's protocol. For RNA-seq library preparation, RNA was further purified by
541 on-column DNase digestion (Qiagen).
542
543 **RNA-seq analysis**
544 RNA quality was evaluated using a Qubit RNA IQ Assay Kit with a Qubit 4 Fluorometer
545 (Thermo Fisher Scientific, Tokyo, Japan). Samples with RNA IQ scores of 9.5–10.0 were
546 used for RNA-seq. cDNA libraries were prepared with the NEBNext Ultra II Directional
547 RNA Library Prep Kit (E7760S, New England Biolabs, Ipswich, MA, USA), SPRIselect
548 (B23317, Beckman Coulter), the NEBNext Poly(A) mRNA Magnetic Isolation Module
549 (E7490S, New England Biolabs), and NEBNext Multiplex Oligos for Illumina (E7710S,
550 New England Biolabs), with all steps following the manufacturer's instructions. Libraries
551 were sequenced on a NextSeq 500 (Illumina, San Diego, CA, USA), and bcl files were
552 converted to fastq using bcl2fastq (Illumina). Reads were analyzed as described by
553 Notaguchi *et al*. (2014) and mapped to the *Arabidopsis* reference (TAIR10) using Bowtie
554 (Langmead et al., 2009) with the options "--all --best --strata." For normalization, read
555 count data were transformed with rlog and adjusted by subtracting the average expression
556 for each gene using default settings of iDEP v0.96 (Ge et al., 2018). DEGs were extracted
557 using edgeR with a false discovery rate cutoff of 0.15 under the default settings of
558 RNAseqChef v1.1.4 (Etoh et al., 2023). Gene set enrichment was performed using
559 ShinyGO v0.82 (Ge et al., 2020) using the default parameters. During analysis we focused
560 on the Biological Process annotation category.
561
562 **Reverse transcription and quantitative RT-PCR**
563 Reverse transcription was performed with the ReverTraAce qPCR RT Master Mix with
564 gDNA Remover (Toyobo, Osaka, Japan). For each reaction, 0.5 µg of RNA was used as
565 input. Synthesized cDNA was diluted five-fold with sterile water and used as template
566 for qRT-PCR. Reactions were run on a QuantStudio 1 system (Thermo Fisher Scientific)
567 using a KOD SYBR qPCR Mix (Toyobo). Relative expression was determined using the
568 comparative Ct method. *TIP41* was used as an internal reference gene. Primer sequences
569 are listed in Supplementary Table S9.
570
571 **Determination of nutrient elements**

572 Shoots were harvested and oven-dried at 80°C for 2 days, ground with a spoon, then
573 stored in a desiccator with silica gel. For carbon and nitrogen quantification, we weighed
574 portions of dried samples, packed them into tin capsules, and subjected them to
575 quantitative analysis using a vario MICRO cube elemental analyzer (Elementar
576 Analysensysteme GmbH, Hanau, Germany). For other elements (e.g., potassium, calcium,
577 sulfur, phosphorus, magnesium, sodium, manganese, zinc, iron, boron, copper,
578 molybdenum, and cobalt), weighed portions of dried samples were digested with HNO_3
579 followed by H_2O_2. Digests were suspended in 1 mL of 0.08 M HNO_3, diluted tenfold with
580 0.08 M HNO_3, and analyzed using inductively coupled plasma mass spectrometry
581 (Agilent 7800 ICP-MS; Agilent Technologies, Santa Clara, CA, USA). Here, indium was
582 used as an internal standard.
583
584 **Nitrate level determination**
585 Nitrate was extracted using 10 volumes of sterile water at 100°C for 20 min. A 5.0 µL
586 aliquot of supernatant was mixed with 40 µL of 5% (w/v) salicylic acid in concentrated
587 sulfuric acid and incubated at room temperature for 20 min. A mock treatment with 40
588 µL concentrated sulfuric acid was prepared in parallel. Finally, 1 mL of 8% (w/v) NaOH
589 was added to the mixture, and nitrate concentrations was determined by recording sample
590 absorbance at 410 nm.
591
592 **Fluorescence microscopy**
593 Fluorescence imaging was performed using an all-in-one fluorescence microscope (BZ-
594 X710, KEYENCE, Osaka, Japan) equipped with a 4× objective (CFI Plan Fluor DL
595 4×/0.13, Nikon, Tokyo, Japan) and a metal halide lamp (No. 91056, KEYENCE). A
596 narrow-band GFP filter (Ex. 480/20; Em. 510/20; 49020, Chroma, Brattleboro, VT, USA)
597 was used for GFP detection, and a Cy5 filter (Ex. 620/60; Em. 700/75; 49006, Chroma)
598 was used for chlorophyll autofluorescence.
599
600 **Leaf cellular analysis**
601 The fifth true leaf was excised from the shoot and scanned at 600 dpi (GT-X980; EPSON)
602 to measure total leaf area. The abaxial surface was pressed onto Scotch transparent
603 adhesive tape (Code: 500-3-15-10P; 3M Japan, Tokyo, Japan) and carefully peeled to

604 isolate epidermal cells. Epidermal cell images were captured using a fluorescence
605 microscope (BZ-X710; KEYENCE) equipped with a 20× objective (CFI Plan Apo
606 20×/0.75; Nikon) and a metal halide lamp (No. 91056, KEYENCE). Thirty epidermal
607 cells were randomly selected, and their areas were measured using ImageJ v1.53t (US
608 National Institutes of Health, Bethesda). The mean area of 30 cells was defined as
609 epidermal cell size. The total epidermal cell number was estimated by dividing the total
610 leaf area by the mean cell size.
611
612 **Statistical analyses**
613 Data were analyzed using unpaired two-tailed Welch's *t*-tests and Dunnett's multiple
614 comparisons tests. All statistical analyses were conducted in R v4.3.0 (R Foundation for
615 Statistical Computing, Vienna, Austria).
616
617 **Data Availability Statement**
618 RNA-seq raw data are deposited in ArrayExpress under accession number E-MTAB-
619 15416.
620
621 **Acknowledgements**
622 We thank Dr. Ryo Tabata and Dr. Tomoko Niwa for technical advice, Ms. Maki Saiki for
623 ICP-MS analysis, and Prof. Thomas Schmülling for important input. We also
624 acknowledge the use of ChatGPT, an AI-based language tool, for support in clarifying
625 the manuscript, and Enago (www.enago.jp) for English language review.
626
627 **Author contributions**
628 K.M. and T.H. conceived and designed experiments. K.M., T.S., M.K., Y.T., T.Ka., H.S.,
629 and T.H. performed the experiments and data analysis. T.Ki., T.N., and T.H. supervised
630 the study. K.M. wrote the manuscript with contributions from all authors. All authors
631 approved the final manuscript.
632
633 **Conflicts of interest**
634 The authors declare that they have no competing interests.
635

Funding

This study was supported by grants from JSPS KAKENHI [No. JP24KJ1709 to K.M., No. 21H02087 to T.Ka., and Nos. 20K05771 and 23K04978 to T.H.] and from JST SPRING [No. JPMJSP2155 to K.M.].

REFERENCES

Abualia R, Ötvös K, Novák O, Bouguyon E, Domanegg K, Krapp A, Nacry P, Gojon A, Lacombe B, Benková E. Molecular framework integrating nitrate sensing in root and auxin-guided shoot adaptive responses. *Proc Natl Acad Sci U S A.* 2022:119(31):e2122460119. 10.1073/pnas.2122460119

Antoniadi I, Novák O, Gelová Z, Johnson A, Plíhal O, Simerský R, Mik V, Vain T, Mateo-Bonmatí E, Karady M, et al. Cell-surface receptors enable perception of extracellular cytokinins. *Nat Commun.* 2020:11(1):4284. 10.1038/s41467-020-17700-9

Arnaud D, Lee S, Takebayashi Y, Choi D, Choi J, Sakakibara H, Hwang I. Cytokinin-mediated regulation of reactive oxygen species homeostasis modulates stomatal immunity in Arabidopsis. *Plant Cell.* 2017:29(3):543–559. 10.1105/tpc.16.00583

Bartrina I, Otto E, Strnad M, Werner T, Schmülling T. Cytokinin regulates the activity of reproductive meristems, flower organ size, ovule formation, and thus seed yield in Arabidopsis thaliana. *Plant Cell.* 2011:23(1):69–80. 10.1105/tpc.110.079079

Bartrina I, Werner S, Schenke A, Gasperini D, Werner T, Schmülling T. Root-derived cytokinin regulates Arabidopsis flowering time through components of the age pathway. *Plant Physiol.* 2025:198(3). 10.1093/plphys/kiaf204

Bhargava A, Clabaugh I, To JP, Maxwell BB, Chiang YH, Schaller GE, Loraine A, Kieber JJ. Identification of cytokinin-responsive genes using microarray meta-analysis and RNA-Seq in Arabidopsis. *Plant Physiol.* 2013:162(1):272–294. 10.1104/pp.113.217026

Caesar K, Thamm AMK, Witthöft J, Elgass K, Huppenberger P, Grefen C, Horak J, Harter K. Evidence for the localization of the Arabidopsis cytokinin receptors AHK3 and AHK4 in the endoplasmic reticulum. *J Exp Bot.* 2011:62(15):5571–5580. 10.1093/jxb/err238

Etoh K, Nakao M. A web-based integrative transcriptome analysis, RNAseqChef, uncovers the cell/tissue type-dependent action of sulforaphane. *J. Biol. Chem.* 2023:299(6):104810. 10.1016/j.jbc.2023.104810

Frank M, Cortleven A, Novák O, Schmülling T. Root-derived trans-zeatin cytokinin protects Arabidopsis plants against photoperiod stress. *Plant Cell Environ.* 2020:43:2637–2649. 10.1111/pce.13860

Frébort I, Kowalska M, Hluska T, Frébortová J, Galuszka P. Evolution of cytokinin biosynthesis and degradation. *J Exp Bot.* 2011:62(8):2431–2452. 10.1093/jxb/err004

Galuszka P, Popelková H, Werner T, Frébortová J, Pospíšilová H, Mik V, Köllmer I, Schmülling T, Frébort I. Biochemical characterization of cytokinin oxidases/dehydrogenases from Arabidopsis thaliana expressed in Nicotiana tabacum L. *J Plant Growth Regul.* 2007:26(3):255–267. 10.1007/s00344-007-9008-5

Gautrat P, Buti S, Romanowski A, Lammers M, Matton SEA, Buijs G, Pierik R. Phytochrome-dependent responsiveness to root-derived cytokinins enables coordinated elongation responses to combined light and nitrate cues. *Nat Commun.* 2024:15:8489. 10.1038/s41467-024-52828-y

Ge SX, Son EW, Yao R. iDEP: an integrated web application for differential expression and pathway analysis of RNA-Seq data. *BMC Bioinformatics.* 2018:19:534. 10.1186/s12859-018-2486-6

Ge SX, Jung D, Yao R. ShinyGO: a graphical gene-set enrichment tool for animals and plants. *Bioinformatics.* 2020:36(8):2628–2629. 10.1093/bioinformatics/btz931

Hachiya T, Oya T, Monden K, Nagae A, Nakagawa T. A cellophane-supported Arabidopsis culture for seamless transfer between different media is useful for studying various nitrogen responses. *Soil Sci. Plant Nutr.* 2021:67(3):277–282. 10.1080/00380768.2021.1908094

Higuchi M, Pischke MS, Mähönen AP, Miyawaki K, Hashimoto Y, Seki M, Kobayashi M, Shinozaki K, Kato T, Tabata S, et al. In planta functions of the Arabidopsis cytokinin receptor family. *Proc Natl Acad Sci U S A.* 2004:101(23):8821–8826. 10.1073/pnas.0402887101

Hirose N, Takei K, Kuroha T, Kamada-Nobusada T, Hayashi H, Sakakibara H. Regulation of cytokinin biosynthesis, compartmentalization and translocation. *J Exp Bot.* 2008:59(1):75–83. 10.1093/jxb/erm157

Hošek P, Hoyerová K, Kiran NS, Dobrev PI, Zahajská L, Filepová R, Motyka V, Müller K, Kamínek M. Distinct metabolism of N-glucosides of isopentenyladenine and trans-zeatin determines cytokinin metabolic spectrum in Arabidopsis. *New Phytol.* 2020:225(6):2423‑2438. 10.1111/nph.16310

Hutchison CE, Kieber JJ. Cytokinin signaling in Arabidopsis. *Plant Cell*. 2002:14(suppl_1):S47–S59. 10.1105/tpc.010444

Inoue T, Higuchi M, Hashimoto Y, Seki M, Kobayashi M, Kato T, Tabata S, Shinozaki K, Kakimoto T. Identification of CRE1 as a cytokinin receptor from Arabidopsis. *Nature.* 2001:409(6823):1060–1063. 10.1038/35059117

Jin SH, Ma XM, Kojima M, Sakakibara H, Wang YW, Hou BK. Overexpression of glucosyltransferase UGT85A1 influences trans-zeatin homeostasis and trans-zeatin responses likely through O-glucosylation. *Planta*. 2013:237(4):991–999. 10.1007/s00425-012-1818-4

Kiba T, Takei K, Kojima M, Sakakibara H. Side-chain modification of cytokinins controls shoot growth in Arabidopsis. *Dev Cell.* 2013:27(4):452–461. 10.1016/j.devcel.2013.10.004

Kiba T, Inaba J, Kudo T, Ueda N, Konishi M, Mitsuda N, Takiguchi Y, Kondou Y, Yoshizumi T, Ohme-Takagi M, et al. Repression of nitrogen starvation responses by members of the Arabidopsis GARP-type transcription factor NIGT1/HRS1 subfamily. *Plant Cell.* 2018:30(4):925–945. 10.1105/tpc.17.00810

Kim HJ, Ryu H, Hong SH, Woo HR, Lim PO, Lee IC, Sheen J, Nam HG, Hwang I. Cytokinin-mediated control of leaf longevity by AHK3 through phosphorylation of ARR2 in Arabidopsis. *Proc Natl Acad Sci U S A.* 2006:103(3):814–819. 10.1073/pnas.0505150103

Ko D, Kang J, Kiba T, Park J, Kojima M, Do J, Kim KY, Kwon M, Endler A, Song W-Y, et al. Arabidopsis ABCG14 is essential for the root-to-shoot translocation of cytokinin. *Proc Natl Acad Sci USA.* 2014:111(19):7150–7155. 10.1073/pnas.1321519111

Kojima M, Kamada-Nobusada T, Komatsu H, Takei K, Kuroha T, Mizutani M, Ashikari M, Ueguchi-Tanaka M, Matsuoka M, Suzuki K, et al. Highly sensitive and high-throughput analysis of plant hormones using MS-probe modification and liquid chromatographytandem mass spectrometry: an application for hormone profiling in Oryza sativa. *Plant Cell Physiol.* 2009:50(7):1201–1214. 10.1093/pcp/pcp057

Kubiasová K, Montesinos JC, Šamajová O, Nisler J, Mik V, Semerádová H, Plíhalová L, Novák O, Marhavý P, Cavallari N, et al. Cytokinin fluoroprobe reveals multiple sites of cytokinin perception at plasma membrane and endoplasmic reticulum. *Nat Commun.* 2020:11(1):4285. 10.1038/s41467-020-17949-0

761 Kurakawa T, Ueda N, Maekawa M, Kobayashi K, Kojima M, Nagato Y, Sakakibara H,
762 Kyozuka J. Direct control of shoot meristem activity by a cytokinin-activating enzyme.
763 *Nature.* 2007:445(7128):652–655. 10.1038/nature05504
764
765 Kuroha T, Tokunaga H, Kojima M, Ueda N, Ishida T, Nagawa S, Fukuda H, Sugimoto
766 K, Sakakibara H. Functional analyses of LONELY GUY cytokinin-activating enzymes
767 reveal the importance of the direct activation pathway in Arabidopsis. *Plant Cell.*
768 2009:21(10):3152–3169. 10.1105/tpc.109.068676
769
770 Landrein B, Formosa-Jordan P, Malivert A, Schuster C, Melnyk CW, Yang W, Turnbull
771 C, Meyerowitz EM, Locke JCW, Jönsson H. Nitrate modulates stem cell dynamics in
772 Arabidopsis shoot meristems through cytokinins. *Proc Natl Acad Sci U S A.*
773 2018:115(6):1382–1387. 10.1073/pnas.1718670115
774
775 Langmead B, Trapnell C, Pop M, Salzberg SL. Ultrafast and memory-efficient alignment
776 of short DNA sequences to the human genome. *Genome Biol.* 2009:10(3):R25.
777 10.1186/gb-2009-10-3-r25
778
779 Liu KH, Liu M, Lin Z, Wang ZF, Chen B, Liu C, Guo A, Konishi M, Yanagisawa S,
780 Wagner G, et al. NIN-like protein 7 transcription factor is a plant nitrate sensor. *Science.*
781 2022:377(6613):1419–1425. 10.1126/science.add1104
782
783 Maeda Y, Konishi M, Kiba T, Sakuraba Y, Sawaki N, Kurai T, Ueda Y, Sakakibara H,
784 Yanagisawa S. A NIGT1-centred transcriptional cascade regulates nitrate signalling and
785 incorporates phosphorus starvation signals in Arabidopsis. *Nat Commun.* 2018:9(1):1376.
786 10.1038/s41467-018-03832-6
787
788 Matsumoto-Kitano M, Kusumoto T, Tarkowski P, Kinoshita-Tsujimura K, Václavíková
789 K, Miyawaki K, Kakimoto T. Cytokinins are central regulators of cambial activity. *Proc*
790 *Natl Acad Sci USA.* 2008:105(50):20027–20031. 10.1073/pnas.0805619105
791

792 Miyawaki K, Matsumoto-Kitano M, Kakimoto T. Expression of cytokinin biosynthetic
793 isopentyltransferase genes in Arabidopsis: tissue specificity and regulation by auxin,
794 cytokinin, and nitrate. *Plant J.* 2004:37(1):128–138. 10.1046/j.1365-313X.2003.01945.x
795
796 Miyawaki K, Tarkowski P, Matsumoto-Kitano M, Kato T, Sato S, Tarkowska D, Tabata
797 S, Sandberg G, Kakimoto T. Roles of Arabidopsis ATP/ADP isopentenyltransferases and
798 tRNA isopentenyltransferases in cytokinin biosynthesis. *Proc Natl Acad Sci USA.*
799 2006:103(44):16598–16603. 10.1073/pnas.0603522103
800
801 Monden K, Kojima M, Takebayashi Y, Suzuki T, Nakagawa T, Sakakibara H, Hachiya
802 T. Root-specific Reduction of Cytokinin Perception Enhances Shoot Growth in
803 Arabidopsis thaliana. *Plant Cell Physiol.* 2022:63(4):484–493. 10.1093/pcp/pcac013
804
805 Müller B, Sheen J. Arabidopsis Cytokinin Signaling Pathway. *Sci. STKE.* 2007:407:cm5.
806 10.1126/stke.4072007cm5
807
808 Nam YJ, Tran LS, Kojima M, Sakakibara H, Nishiyama R, Shin R. Regulatory roles of
809 cytokinins and cytokinin signaling in response to potassium deficiency in Arabidopsis.
810 *PLoS One*. 2012:7(10): e47797. 10.1371/journal.pone.0047797
811
812 Niemann MCE, Weber H, Hluska T, Leonte G, Anderson SM, Novak O, Senes A, Werner
813 T. The cytokinin oxidase/dehydrogenase CKX1 is a membrane-bound protein requiring
814 homooligomerization in the endoplasmic reticulum for its cellular activity. *Plant Physiol.*
815 2018:176(3):2024–2039. 10.1104/pp.17.00925
816
817 Notaguchi M, Higashiyama T, Suzuki T. Identification of mRNAs that move over long
818 distances using an RNA-Seq analysis of Arabidopsis/Nicotiana benthamiana heterografts.
819 *Plant Cell Physiol.* 2015:56(2):311–321. 10.1093/pcp/pcu210
820
821 Osugi A, Kojima M, Takebayashi Y, Ueda N, Kiba T, Sakakibara H. Systemic transport
822 of trans-zeatin and its precursor have differing roles in Arabidopsis shoots. *Nat Plants.*
823 2017:3:17112. 10.1038/nplants.2017.112

Rahayu YS, Walch-Liu P, Neumann G, Römheld V, von Wirén N, Bangerth F. Root-derived cytokinins as long-distance signals for NO3−-induced stimulation of leaf growth. *J Exp Bot.* 2005:56(414):1143–1152. 10.1093/jxb/eri107

Riefler M, Novak O, Strnad M, Schmülling T. Arabidopsis cytokinin receptor mutants reveal functions in shoot growth, leaf senescence, seed size, germination, root development, and cytokinin metabolism. *Plant Cell.* 2006:18(1):40–54. 10.1105/tpc.105.037796

Romanov GA, Lomin SN, Schmülling T. Biochemical characteristics and ligand-binding properties of Arabidopsis cytokinin receptor AHK3 compared to CRE1/AHK4 as revealed by a direct binding assay. *J Exp Bot.* 2006:57(15):4051–4058. 10.1093/jxb/erl179

Sakakibara H, Suzuki M, Takei K, Deji A, Taniguchi M, Sugiyama T. A response‐regulator homologue possibly involved in nitrogen signal transduction mediated by cytokinin in maize. *Plant J.* 1998:14:337‐344. 10.1046/j.1365-313X.1998.00134.x

Sakakibara H, Takei K, Hirose N. Interactions between nitrogen and cytokinin in the regulation of metabolism and development. *Trends Plant Sci.* 2006:11: 440–448. 10.1016/j.tplants.2006.07.004

Sakakibara H. Cytokinin biosynthesis and transport for systemic nitrogen signaling. *Plant J.* 2021:105(2):421–430. 10.1111/tpj.15011

Sakakibara H. Five unaddressed questions about cytokinin biosynthesis. *J. Exp. Bot.* 2025:76(7):1941–1949. 10.1093/jxb/erae348

853 Schmülling T, Werner T, Riefler M, Krupková E, Bartrina y Manns I. Structure and
854 function of cytokinin oxidase/dehydrogenase genes of maize, rice, Arabidopsis and other
855 species. *J Plant Res.* 2003:116:241–252. 10.1007/s10265-003-0096-4
856
857 Spichal L, Rakova NY, Riefler M, Mizuno T, Romanov GA, Strnad M, Schmülling T.
858 Two cytokinin receptors of Arabidopsis thaliana, CRE1/AHK4 and AHK3, differ in their
859 ligand specificity in a bacterial assay. *Plant Cell Physiol.* 2004:45(9):1299–1305.
860 10.1093/pcp/pch132
861
862 Stolz A, Riefler M, Lomin SN, Achazi K, Romanov GA, Schmülling T. The specificity
863 of cytokinin signalling in Arabidopsis thaliana is mediated by differing ligand affinities
864 and expression profiles of the receptors. *Plant J.* 2011:67(1):157–168. 10.1111/j.1365-
865 313X.2011.04584.x
866
867 Takei K, Sakakibara H, Sugiyama T. Identification of genes encoding adenylate
868 isopentenyltransferase, a cytokinin biosynthesis enzyme, in Arabidopsis thaliana. *J Biol*
869 *Chem.* 2001a:276(28):26405–26410. 10.1074/jbc.M102130200
870
871 Takei K, Sakakibara H, Taniguchi M, Sugiyama T. Nitrogen-dependent accumulation of
872 cytokinins in root and the translocation to leaf: Implication of cytokinin species that
873 induces gene expression of maize response regulator. *Plant Cell Physiol.*
874 2001b:42(1):85–93. 10.1093/pcp/pce009
875
876 Takei K, Yamaya T, Sakakibara H. Arabidopsis CYP735A1 and CYP735A2 encode
877 cytokinin hydroxylases that catalyze the biosynthesis of trans-zeatin. *J Biol Chem.*
878 2004a:279(40):41866–41872. 10.1074/jbc.M406337200
879
880 Takei K, Ueda N, Aoki K, Kuromori T, Hirayama T, Shinozaki K, Yamaya T, Sakakibara
881 H. AtIPT3 is a key determinant of nitrate-dependent cytokinin biosynthesis in
882 Arabidopsis. *Plant Cell Physiol.* 2004b:45(8):1053–1062. 10.1093/pcp/pch119
883

To JPC, Haberer G, Ferreira FJ, Deruère J, Mason MG, Schaller GE, Alonso JM, Ecker JR, Kieber JJ. Type-A ARRs are partially redundant negative regulators of cytokinin signaling in Arabidopsis. *Plant Cell.* 2004:16(3):658–671. 10.1105/tpc.018978

Wang J, Ma XM, Kojima M, Sakakibara H, Hou BK. N-Glucosyltransferase UGT76C2 is involved in cytokinin homeostasis and cytokinin response in Arabidopsis thaliana. *Plant Cell Physiol*. 2011:52 (12):2200–2213. 10.1093/pcp/pcr152

Wang J, Ma XM, Kojima M, Sakakibara H, Hou BK. Glucosyltransferase UGT76C1 finely modulates cytokinin responses via cytokinin N-glucosylation in Arabidopsis thaliana. *Plant Physiol. Biochem*. 2013:65:9–16. 10.1016/j.plaphy.2013.01.012

Werner T, Motyka V, Strnad M, Schmülling T. Regulation of plant growth by cytokinin. *Proc. Natl. Acad. Sci. USA.* 2001:98(18):10487–10492. 10.1073/pnas.171304098

Werner T, Motyka V, Laucou V, Smets R, Van Onckelen H, Schmülling T. Cytokinin-deficient transgenic Arabidopsis plants show multiple developmental alterations indicating opposite functions of cytokinins in the regulation of shoot and root meristem activity. *Plant Cell.* 2003:15(11):2532–2550. 10.1105/tpc.014928

Werner T, Köllmer I, Bartrina I, Holst K, Schmülling T. New insights into the biology of cytokinin degradation. *Plant Biol.* 2006:8(3):371–381. 10.1055/s-2006-923928

Wulfetange K, Lomin SN, Romanov GA, Stolz A, Heyl A, Schmülling T. The cytokinin receptors of Arabidopsis are located mainly to the endoplasmic reticulum. *Plant Physiol.* 2011:156(4):1808–1818. 10.1104/pp.111.180539

Zhang K, Novak O, Wei Z, Gou M, Zhang X, Yu Y, Yang H, Cai Y, Strnad M, Liu CJ. Arabidopsis ABCG14 protein controls the acropetal translocation of root-synthesized cytokinins. *Nat Commun.* 2014:5(1):3274. 10.1038/ncomms4274

915 Zhao J, Ding B, Zhu E, Deng X, Zhang M, Zhang P, Wang L, Dai Y, Xiao S, Zhang C,
916 et al. Phloem unloading via the apoplastic pathway is essential for shoot distribution of
917 root-synthesized cytokinins. *Plant Physiol.* 2021:186(4):2111–2123.
918 10.1093/plphys/kiab188
919
920 Zhao J, Deng X, Qian J, Liu T, Ju M, Li J, Yang Q, Zhu X, Li W, Liu C-J, et al.
921 Arabidopsis ABCG14 forms a homodimeric transporter for multiple cytokinins and
922 mediates long-distance transport of isopentenyladenine-type cytokinins. *Plant Commun.*
923 2023:4(2):100468. 10.1016/j.xplc.2022.100468
924
925 Zürcher E, Tavor-Deslex D, Lituiev D, Enkerli K, Tarr PT, Müller B. A robust and
926 sensitive synthetic sensor to monitor the transcriptional output of the cytokinin signaling
927 network in planta. *Plant Physiol.* 2013:161(3):1066–1075. 10.1104/pp.112.211763
928
929 **FIGURE LEGENDS**
930 **Figure 1. Effects of root-specific CK receptor deficiency on shoot growth in medium.**
931 (A) Representative shoots of grafted plants. Scale bars = 5 mm. (B–D) Shoot fresh weight
932 (B), leaf blade area (C), and leaf number (D) of grafted plants. Data pooled from two
933 independent grafting experiments are shown as mean ± SD (n = 12). Asterisks indicate
934 significant differences relative to WT/WT (**P* < 0.05, ***P* < 0.01, ****P* < 0.001;
935 Dunnett's test). Numbers on graphs show mean values relative to WT/WT (set = 1).
936 Grafted plants are denoted as "scion line/rootstock line." WT, Col-0; *a2*, *ahk2-5*; *a3*,
937 *ahk3-7*; *a4*, *cre1-2*; *a23*, *ahk2-5 ahk3-7*; *a24*, *ahk2-5 cre1-2*; *a34*, *ahk3-7 cre1-2*.
938
939 **Figure 2. Effects of root-specific CK receptor deficiency on root CK concentration.**
940 (A–B) Root concentrations of active form iP and *t*Z and their precursors (A), and inactive
941 form iP- and *t*Z-type CKs (B) in grafted plants. Data are pooled from three independent
942 grafting experiments and are reported as mean ± SD (n = 3). Asterisks indicate significant
943 differences relative to WT/WT (***P* < 0.01, ****P* < 0.001; Dunnett's test). Grafted plants
944 are denoted as "scion line/rootstock line." WT, Col-0; *a2*, *ahk2-5*; *a3*, *ahk3-7*; *a4*, *cre1-*
945 *2*; FW, fresh weight; *t*Z, *trans*-zeatin; iP, N^6-(Δ^2-isopentenyl) adenine; iP and their
946 precursors = sum of iP, iPR, and iPRPs; inactive form iP-type CKs = sum of iP7G and

947 iP9G; *t*Z and their precursors = sum of *t*Z, *t*ZR, and *t*ZRPs; inactive form *t*Z-type CKs =
948 sum of *t*Z7G, *t*Z9G, *t*ZOG, and *t*ZROG.
949
950 **Figure 3. Effects of root-specific CK receptor deficiency on the root transcriptome.**
951 (A) Volcano plots of DEGs between WT/WT and WT/*ahk2*, WT/*ahk3*, or WT/*ahk4* roots.
952 DEG analysis was performed with RNAseqChef (Etoh et al., 2023) using edgeR, applying
953 a 1.5-fold change threshold and FDR cutoff of 0.15 (all other parameters default). x-axis:
954 $\log_2$ fold change ($\log_2$ FC); y-axis: $-\log_{10}$ adjusted p-value (padj). Each dot represents a
955 single gene. Red, blue, and grey indicate upregulated, downregulated, and non-significant
956 genes, respectively. Log_2 FC was limited to –4 to 4 and padj to ≦50. Full-range volcano
957 plots are provided in Supplementary Fig. S4. (B) Mean normalized transcript levels of
958 CK-inducible and CK-repressible genes (mean ± SD). Gene list obtained from Bhargava
959 *et al*. (2013). (C) Transcriptional changes in CK biosynthesis and inactivation genes,
960 visualized as heatmaps with MORPHEUS (https://software.broadinstitute.org/morpheus)
961 based on $\log_2$-transformed ratios of each graft to WT/WT mean RPM. Color scale: blue
962 (minimum) to yellow (maximum) per row. (D) Root expression of *CKX4* in grafted plants
963 by qRT-PCR. Relative transcript levels were normalized to the WT/WT root mean (set =
964 1) and $\log_2$-transformed. Data pooled from two independent grafting experiments are
965 shown as mean ± SD (n = 6). Asterisks indicate significant differences relative to WT/WT
966 (**P < 0.01, ***P < 0.001; Dunnett's test). Grafted plants are denoted as "scion
967 line/rootstock line." WT, Col-0; *a2*, *ahk2-5*; *a3*, *ahk3-7*; *a4*, *cre1-2*; FC, fold change.
968
969 **Figure 4. Effects of root-specific CK receptor deficiency on CK concentration of**
970 **xylem sap.** (A–B) Xylem sap concentrations of iP- and *t*Z-type CKs (A) and of *t*Z, *t*ZR,
971 and *t*ZRPs (B) in grafted plants. Data pooled from three independent grafting experiments
972 are reported as mean ± SD (n = 3). Asterisks indicate significant differences relative to
973 WT/WT (*P < 0.05, **P < 0.01, ***P < 0.001; Dunnett's test). Grafted plants are denoted
974 as "scion line/rootstock line." WT, Col-0; *a2*, *ahk2-5*; *a3*, *ahk3-7*; *a4*, *cre1-2*; *t*Z, *trans*-
975 zeatin; *t*ZR, *t*Z-riboside; *t*ZRPs, *t*ZR 5′-phosphates; iP-type CKs = sum of iPR, iPRPs,
976 and iP7G; *t*Z-type CKs = sum of *t*Z, *t*ZR, *t*ZRPs, *t*Z7G, *t*Z9G, and *t*ZOG.
977

978 **Figure 5. Effects of root-specific CK receptor deficiency on the shoot transcriptome.**
979 (A) Volcano plots of DEGs between WT/WT and WT/*ahk2*, WT/*ahk3*, or WT/*ahk4*
980 shoots. DEG analysis was performed with RNAseqChef (Etoh et al., 2023) using edgeR,
981 applying a 1.5-fold change threshold and FDR cutoff of 0.15 (default parameters
982 otherwise). x-axis: $\log_2$ fold change ($\log_2$ FC); y-axis: $-\log_{10}$ adjusted p-value (padj). Each
983 dot represents one gene; red, blue, and grey indicate upregulated, downregulated, and
984 non-significant genes, respectively. Log_2 FC values were limited to –4 to 4 and padj
985 values to ≦5. (B) Lollipop plots showing GO enrichment analysis from the 163 genes
986 upregulated in WT/*ahk3* shoots, generated with ShinyGO (Ge et al., 2020) using default
987 settings for biological process terms. (C) Heatmaps of transcriptional changes in type-A
988 *ARR* genes, visualized with MORPHEUS (https://software.broadinstitute.org/morpheus)
989 based on $\log_2$-transformed ratios of each graft to the WT/WT mean RPM. Color scale:
990 blue (minimum) to yellow (maximum) per row. (D) Shoot expression of *ARR5*
991 determined by qRT-PCR. Values were normalized to the WT/WT shoot mean (set = 1)
992 and $\log_2$-transformed. Data pooled from two independent grafting experiments are
993 reported as mean ± SD (n = 6). Asterisks indicate significant differences relative to
994 WT/WT (**P* < 0.05; Dunnett's test). Grafted plants are denoted as "scion line/rootstock
995 line." WT, Col-0; *a2*, *ahk2-5*; *a3*, *ahk3-7*; *a4*, *cre1-2*; FC, fold change.
996
997 **Figure 6. Effects of root-specific *AHK3* deficiency on shoot growth via CK signaling.**
998 (A–E) Shoot fresh weight and leaf blade area in grafted plants: (A) WT/WT, WT/*ahk3*,
999 WT/*abcg14*, and WT/*ahk3 abcg14*; (B) WT/WT, WT/*ahk3*, WT/*cypDM*, and WT/*ahk3*
1000 *cypDM*; (C) WT/WT, WT/*ahk3*, *ahk2*/*ahk3*, *ahk3*/*ahk3*, and *ahk4*/*ahk3*; (D) WT/WT,
1001 WT/*ahk3*, *ahk23*/*ahk3*, *ahk24*/*ahk3*, and *ahk34*/*ahk3*; (E) *TCSn:GFP*/WT and
1002 *TCSn:GFP*/*ahk3*. (F) Representative fluorescent image of the adaxial side of the sixth
1003 true leaf in grafted plants. Green = GFP; red = autofluorescence. Scale bars = 1 mm. GFP
1004 intensity was quantified with ImageJ as the mean signal in the region marked by a white
1005 dashed box. (G) Epidermal cell size and number on the abaxial side of the fifth true leaf.
1006 Data pooled from two independent grafting experiments are reported as mean ± SD (n =
1007 12 (A–E), 11 (F), or 6 (G)). Asterisks (**P* < 0.05, ***P* < 0.01, ****P* < 0.001) indicate
1008 significant differences relative to WT/WT by Dunnett's test. Pairwise differences by

1009 Welch's *t*-test are marked with asterisks above horizontal lines. Graph numbers show
1010 mean values relative to WT/WT (set = 1). Grafted plants are denoted as "scion
1011 line/rootstock line." WT, Col-0; *a2*, *ahk2-5*; *a3*, *ahk3-7*; *a4*, *cre1-2*; *a23*, *ahk2-5 ahk3-7*;
1012 *a24*, *ahk2-5 cre1-2*; *a34*, *ahk3-7 cre1-2*; *g14*, *abcg14*; *DM*, *cyp735a1-2 cyp735a2-2*;
1013 *a3g14*, *ahk3-7 abcg14*; *a3DM*, *ahk3-7 cyp735a1-2 cyp735a2-2*; *TCS*, *TCSn:GFP*; ns, not
1014 significant.
1015
1016 **Figure 7. Effects of root-specific *AHK3* or *CKX4* deficiency on shoot growth in**
1017 **response to nitrate signaling.** (A, B, E) Shoot fresh weight and leaf blade area of grafted
1018 plants 5 days after transfer from 5 mM NH_4^+ medium to either 5 mM NH_4^+ + 0.5 mM
1019 KNO_3 or 5 mM NH_4^+ + 0.5 mM KCl: (A) WT/WT and WT/*ahk3*; (B) WT/WT, WT/*ahk3*,
1020 WT/*abcg14*, and WT/*ahk3 abcg14*; (E) WT/WT, WT/*ckx4-1*, and WT/*ckx4-2*. (C) Root
1021 expression of *IPT3*, *IPT7*, *CYP735A1*, *CYP735A2*, *CKX1*, *CKX3*, *CKX4*, *CKX5*, *CKX6*,
1022 *CKX7*, *UGT76C1*, *UGT76C2*, and *UGT85A1* 4 hours after transfer. Heatmaps were
1023 generated with MORPHEUS (https://software.broadinstitute.org/morpheus) from $\log_2$
1024 fold change values relative to WT/WT under 5 mM NH_4^+ + 0.5 mM KCl (set = 1). Color
1025 scale: blue (minimum) to yellow (maximum) per row. (D) RT-PCR analysis of *CKX4* in
1026 WT, *ckx4-1*, and *ckx4-2* seedlings grown 7 days on 1/2 MS medium. *TIP41* was the
1027 control. Primers are listed in Supplementary Table S8. Data are shown as mean ± SD with
1028 replicates as follows: (A) n = 18, two replicates; (B) n = 18, three replicates; (C) n = 6,
1029 two replicates; (E) n = 24, four replicates. Asterisks (*$P < 0.05$, **$P < 0.01$, ***$P < 0.001$)
1030 mark significant differences relative to WT/WT under 5 mM NH_4^+ + 0.5 mM KCl
1031 (Dunnett's test). Pairwise comparisons used Welch's *t*-tests (A). For multiple treatments
1032 vs. one control, we used Dunnett's tests (B, E). Significant differences are shown by
1033 asterisks above horizontal lines. Graph numbers indicate mean values relative to WT/WT
1034 under 5 mM NH_4^+ + 0.5 mM KCl (set = 1). Grafted plants are denoted as "scion
1035 line/rootstock line." WT, Col-0; *a3*, *ahk3-7*; *g14*, *abcg14*; *a3g14*, *ahk3-7 abcg14*; *c4-1*,
1036 *ckx4-1*; *c4-2*, *ckx4-2*; ns, not significant; KCl, 5 mM NH_4^+ + 0.5 mM KCl; KNO_3, 5 mM
1037 NH_4^+ + 0.5 mM KNO_3.

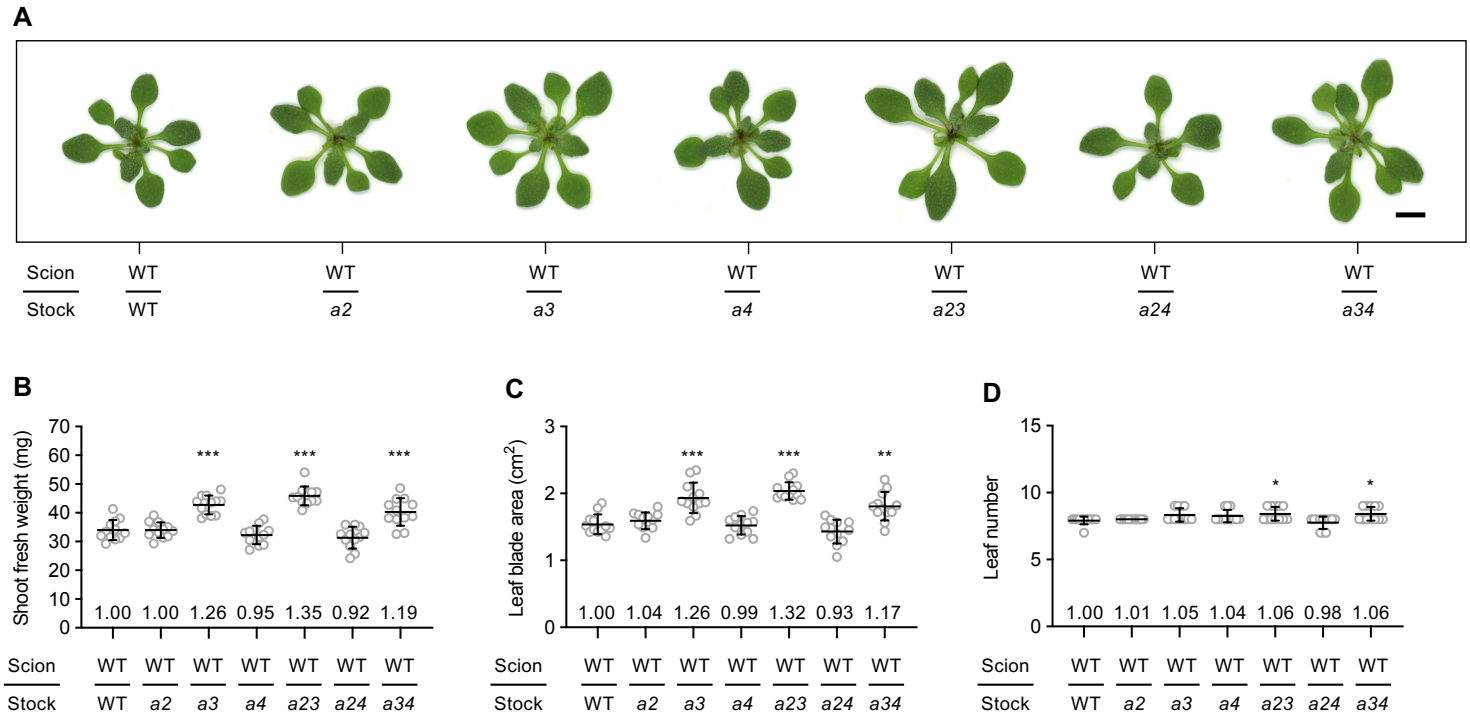

Figure 1. Effects of root-specific CK receptor deficiency on shoot growth in medium. (A) Representative shoots of grafted plants. Scale bars = 5 mm. (B–D) Shoot fresh weight (B), leaf blade area (C), and leaf number (D) of grafted plants. Data pooled from two independent grafting experiments are shown as mean ± SD (n = 12). Asterisks indicate significant differences relative to WT/WT (**P* < 0.05, ***P* < 0.01, ****P* < 0.001; Dunnett's test). Numbers on graphs show mean values relative to WT/WT (set = 1). Grafted plants are denoted as "scion line/rootstock line." WT, Col-0; *a2*, *ahk2-5*; *a3*, *ahk3-7*; *a4*, *cre1-2*; *a23*, *ahk2-5 ahk3-7*; *a24*, *ahk2-5 cre1-2*; *a34*, *ahk3-7 cre1-2*.

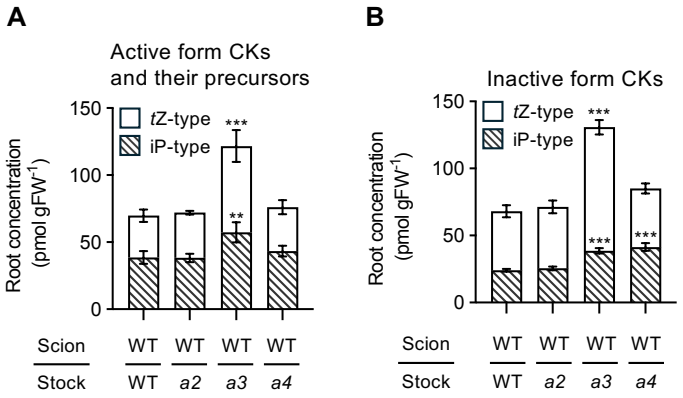

Figure 2. Effects of root-specific CK receptor deficiency on root CK concentration. (A–B) Root concentrations of active form iP and *t*Z and their precursors (A), and inactive form iP- and *t*Z-type CKs (B) in grafted plants. Data are pooled from three independent grafting experiments and are reported as mean ± SD (n = 3). Asterisks indicate significant differences relative to WT/WT (***P* < 0.01, ****P* < 0.001; Dunnett's test). Grafted plants are denoted as "scion line/rootstock line." WT, Col-0; *a2*, *ahk2-5*; *a3*, *ahk3-7*; *a4*, *cre1-2*; FW, fresh weight; *t*Z, *trans*-zeatin; iP, N^6-(Δ^2-isopentenyl) adenine; iP and their precursors = sum of iP, iPR, and iPRPs; inactive form iP-type CKs = sum of iP7G and iP9G; *t*Z and their precursors = sum of *t*Z, *t*ZR, and *t*ZRPs; inactive form *t*Z-type CKs = sum of *t*Z7G, *t*Z9G, *t*ZOG, and *t*ZROG.

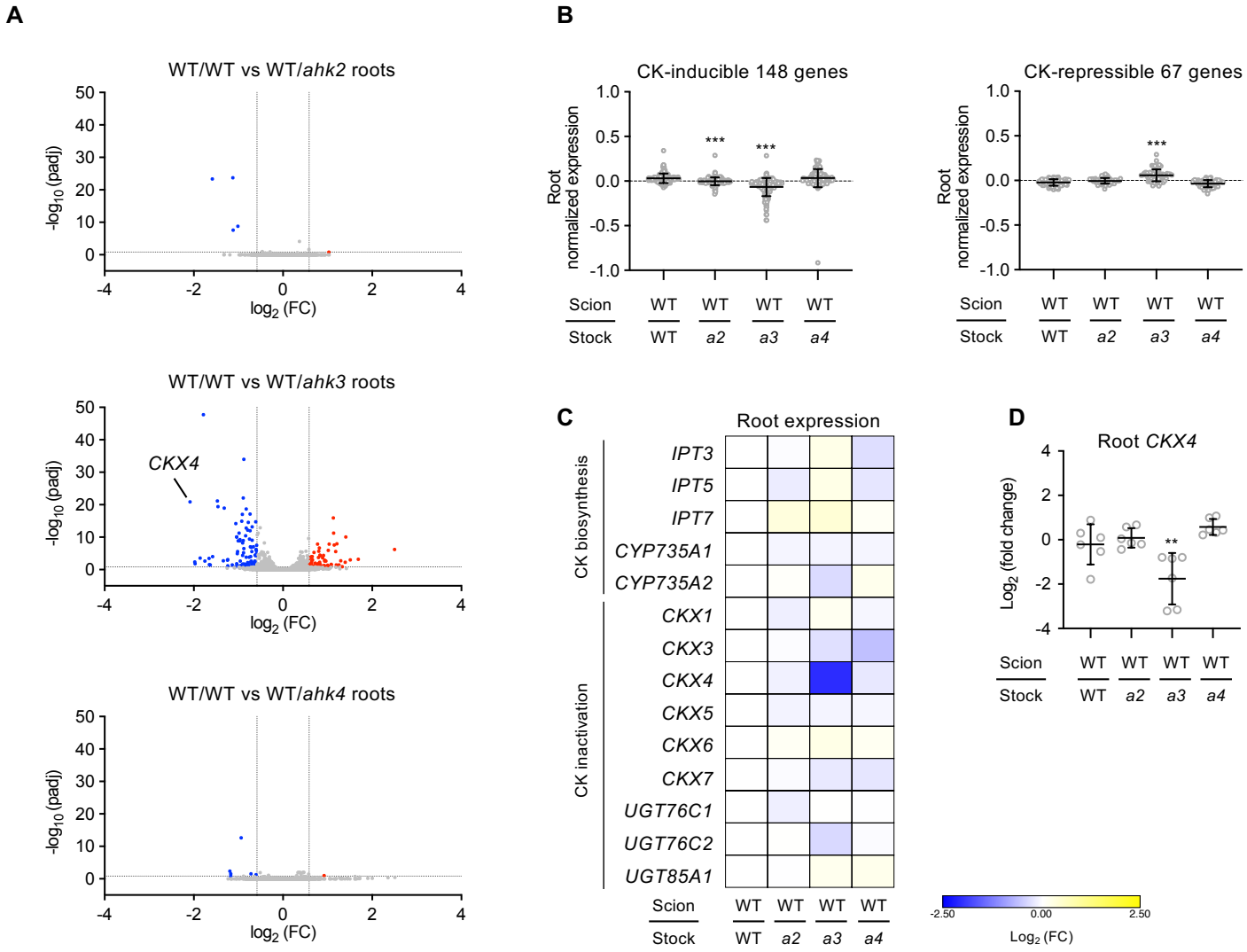

Figure 3. Effects of root-specific CK receptor deficiency on the root transcriptome. (A) Volcano plots of DEGs between WT/WT and WT/*ahk2*, WT/*ahk3*, or WT/*ahk4* roots. DEG analysis was performed with RNAseqChef (Etoh et al., 2023) using edgeR, applying a 1.5-fold change threshold and FDR cutoff of 0.15 (all other parameters default). x-axis: $\log_2$ fold change ($\log_2$ FC); y-axis: $-\log_{10}$ adjusted p-value (padj). Each dot represents a single gene. Red, blue, and grey indicate upregulated, downregulated, and non-significant genes, respectively. Log_2 FC was limited to –4 to 4 and padj to ≦50. Full-range volcano plots are provided in Supplementary Fig. S4. (B) Mean normalized transcript levels of CK-inducible and CK-repressible genes (mean ± SD). Gene list obtained from Bhargava *et al.* (2013). (C) Transcriptional changes in CK biosynthesis and inactivation genes, visualized as heatmaps with MORPHEUS (https://software.broadinstitute.org/morpheus) based on $\log_2$-transformed ratios of each graft to WT/WT mean RPM. Color scale: blue (minimum) to yellow (maximum) per row. (D) Root expression of *CKX4* in grafted plants by qRT-PCR. Relative transcript levels were normalized to the WT/WT root mean (set = 1) and $\log_2$-transformed. Data pooled from two independent grafting experiments are shown as mean ± SD (n = 6). Asterisks indicate significant differences relative to WT/WT (***P* < 0.01, ****P* < 0.001; Dunnett's test). Grafted plants are denoted as "scion line/rootstock line." WT, Col-0; *a2*, *ahk2-5*; *a3*, *ahk3-7*; *a4*, *cre1-2*; FC, fold change.

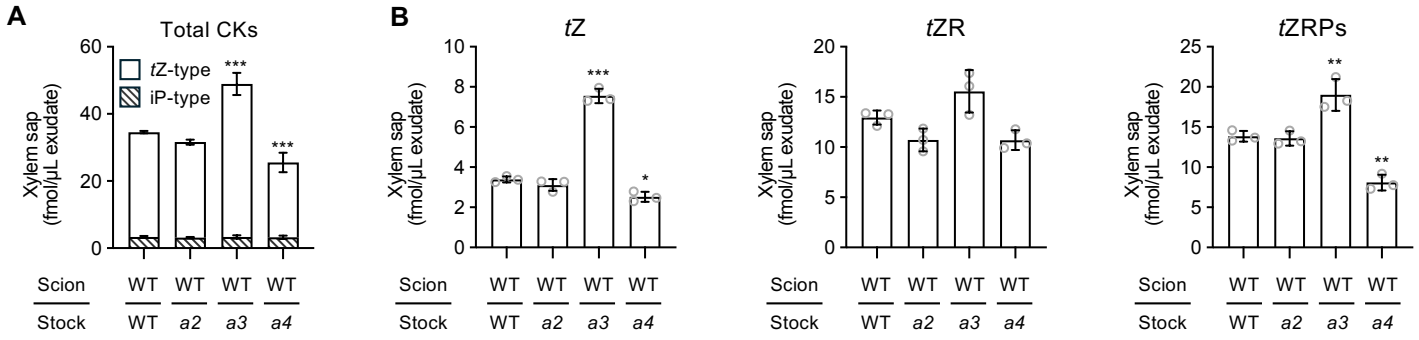

Figure 4. Effects of root-specific CK receptor deficiency on CK concentration of xylem sap. (A–B) Xylem sap concentrations of iP- and *t*Z-type CKs (A) and of *t*Z, *t*ZR, and *t*ZRPs (B) in grafted plants. Data pooled from three independent grafting experiments are reported as mean ± SD (n = 3). Asterisks indicate significant differences relative to WT/WT (**P* < 0.05, ***P* < 0.01, ****P* < 0.001; Dunnett's test). Grafted plants are denoted as "scion line/rootstock line." WT, Col-0; *a2*, *ahk2-5*; *a3*, *ahk3-7*; *a4*, *cre1-2*; *t*Z, *trans*-zeatin; *t*ZR, *t*Z-riboside; *t*ZRPs, *t*ZR 5′-phosphates; iP-type CKs = sum of iPR, iPRPs, and iP7G; *t*Z-type CKs = sum of *t*Z, *t*ZR, *t*ZRPs, *t*Z7G, *t*Z9G, and *t*ZOG.

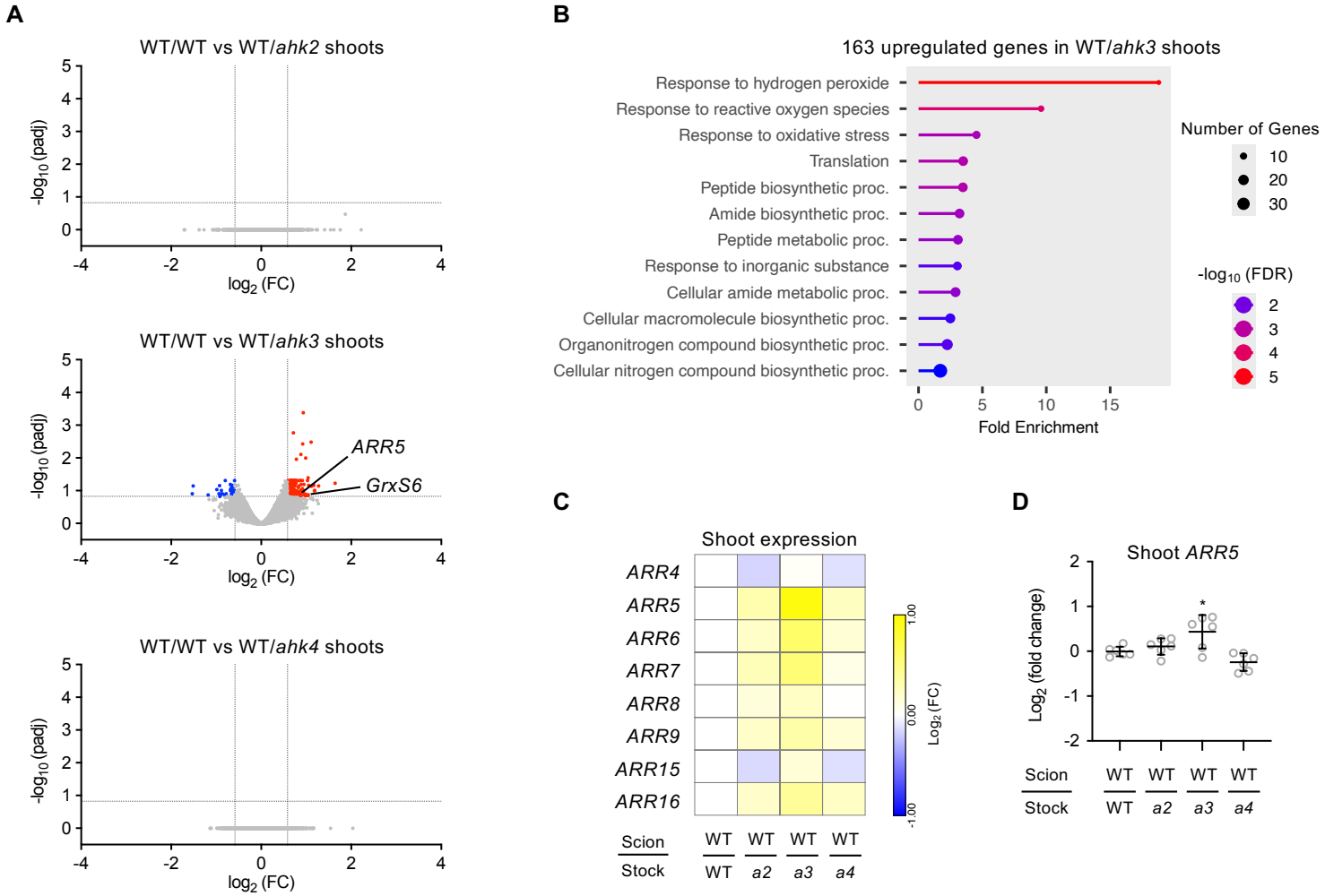

Figure 5. Effects of root-specific CK receptor deficiency on the shoot transcriptome. (A) Volcano plots of DEGs between WT/WT and WT/*ahk2*, WT/*ahk3*, or WT/*ahk4* shoots. DEG analysis was performed with RNAseqChef (Etoh et al., 2023) using edgeR, applying a 1.5-fold change threshold and FDR cutoff of 0.15 (default parameters otherwise). x-axis: $\log_2$ fold change ($\log_2$ FC); y-axis: $-\log_{10}$ adjusted p-value (padj). Each dot represents one gene; red, blue, and grey indicate upregulated, downregulated, and non-significant genes, respectively. (B) Lollipop plots showing GO enrichment analysis from the 163 genes upregulated in WT/*ahk3* shoots, generated with ShinyGO (Ge et al., 2020) using default settings for biological process terms. (C) Heatmaps of transcriptional changes in type-A *ARR* genes, visualized with MORPHEUS (https://software.broadinstitute.org/morpheus) based on $\log_2$-transformed ratios of each graft to the WT/WT mean RPM. Color scale: blue (minimum) to yellow (maximum) per row. (D) Shoot expression of *ARR5* determined by qRT-PCR. Values were normalized to the WT/WT shoot mean (set = 1) and $\log_2$-transformed. Data pooled from two independent grafting experiments are reported as mean ± SD (n = 6). Asterisks indicate significant differences relative to WT/WT (*$P < 0.05$; Dunnett's test). Grafted plants are denoted as "scion line/rootstock line." WT, Col-0; *a2*, *ahk2-5*; *a3*, *ahk3-7*; *a4*, *cre1-2*; FC, fold change.

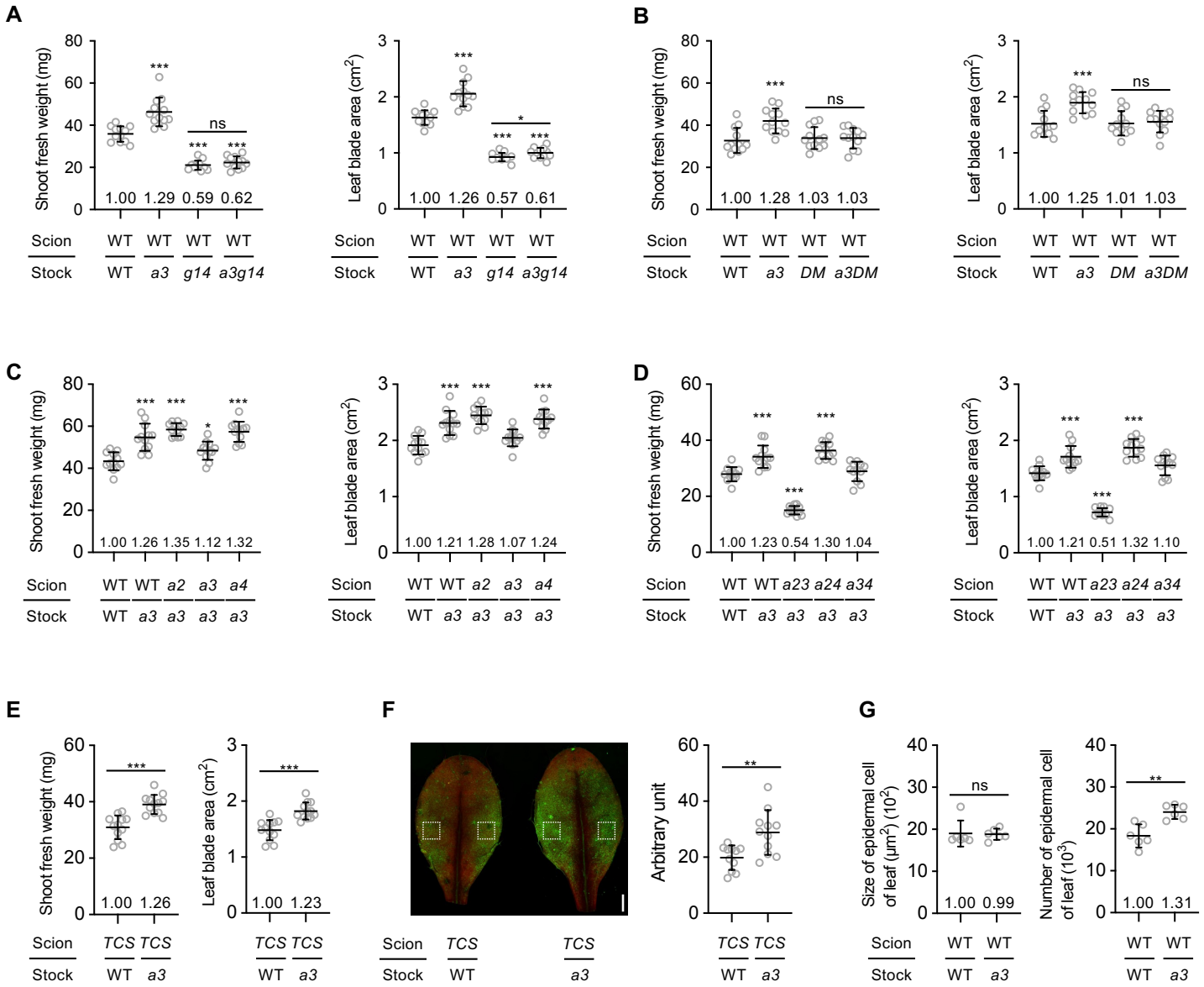

Figure 6. Effects of root-specific *AHK3* deficiency on shoot growth via CK signaling. (A–E) Shoot fresh weight and leaf blade area in grafted plants: (A) WT/WT, WT/*ahk3*, WT/*abcg14*, and WT/*ahk3 abcg14*; (B) WT/WT, WT/*ahk3*, WT/*cypDM*, and WT/*ahk3 cypDM*; (C) WT/WT, WT/*ahk3*, *ahk2*/*ahk3*, *ahk3*/*ahk3*, and *ahk4*/*ahk3*; (D) WT/WT, WT/*ahk3*, *ahk23*/*ahk3*, *ahk24*/*ahk3*, and *ahk34*/*ahk3*; (E) *TCSn:GFP*/WT and *TCSn:GFP*/*ahk3*. (F) Representative fluorescent image of the adaxial side of the sixth true leaf in grafted plants. Green = GFP; red = autofluorescence. Scale bars = 1 mm. GFP intensity was quantified with ImageJ as the mean signal in the region marked by a white dashed box. (G) Epidermal cell size and number on the abaxial side of the fifth true leaf. Data pooled from two independent grafting experiments are reported as mean ± SD (n = 12 (A–E), 11 (F), or 6 (G)). Asterisks (*$P < 0.05$, **$P < 0.01$, ***$P < 0.001$) indicate significant differences relative to WT/WT by Dunnett's test. Pairwise differences by Welch's *t*-test are marked with asterisks above horizontal lines. Graph numbers show mean values relative to WT/WT (set = 1). Grafted plants are denoted as "scion line/rootstock line." WT, Col-0; *a2*, *ahk2-5*; *a3*, *ahk3-7*; *a4*, *cre1-2*; *a23*, *ahk2-5 ahk3-7*; *a24*, *ahk2-5 cre1-2*; *a34*, *ahk3-7 cre1-2*; *g14*, *abcg14*; *DM*, *cyp735a1-2 cyp735a2-2*; *a3g14*, *ahk3-7 abcg14*; *a3DM*, *ahk3-7 cyp735a1-2 cyp735a2-2*; *TCS*, *TCSn:GFP*; ns, not significant.

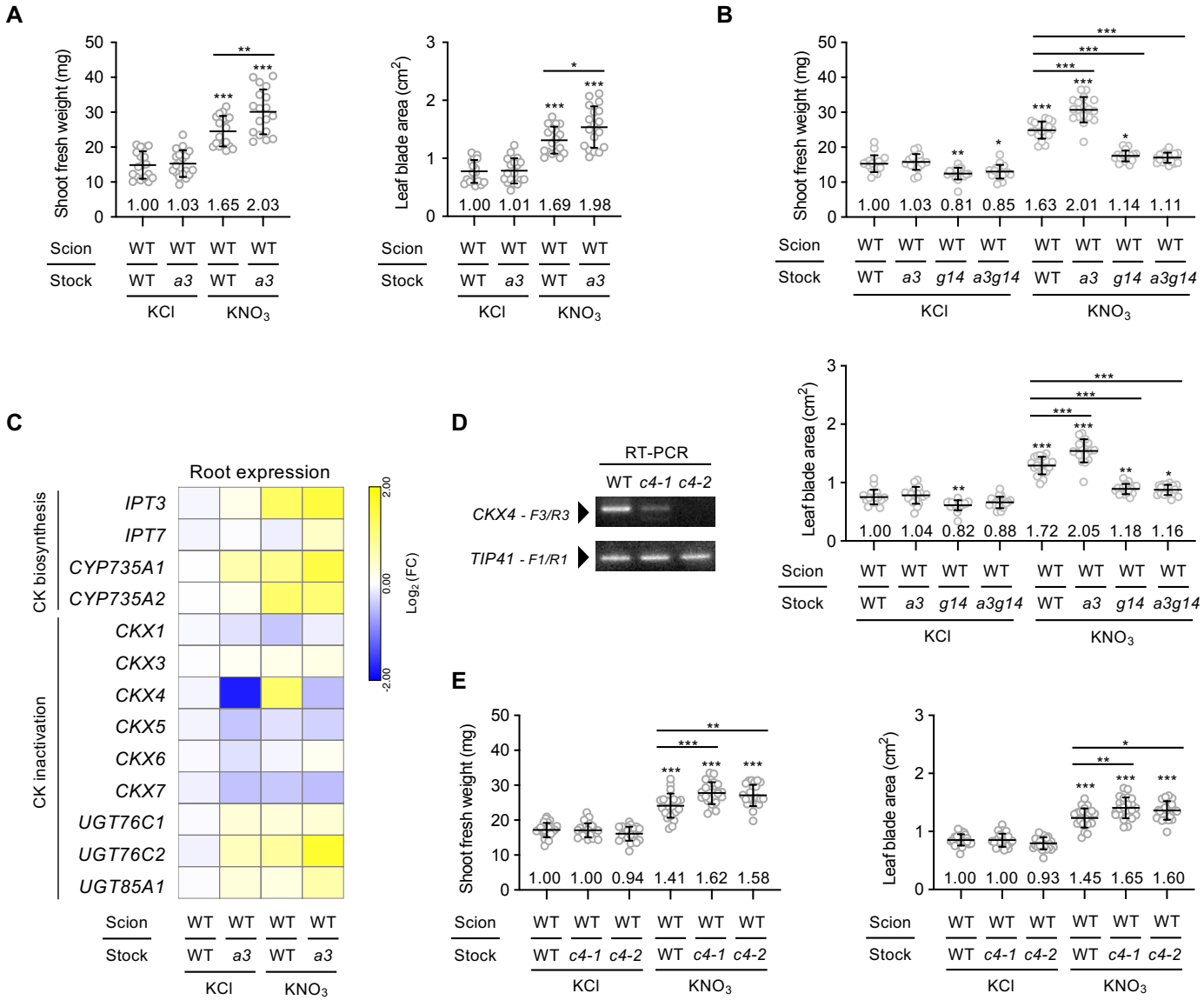

Figure 7. Effects of root-specific *AHK3* or *CKX4* deficiency on shoot growth in response to nitrate signaling. (A, B, E) Shoot fresh weight and leaf blade area of grafted plants 5 days after transfer from 5 mM NH_4^+ medium to either 5 mM NH_4^+ + 0.5 mM KNO_3 or 5 mM NH_4^+ + 0.5 mM KCl: (A) WT/WT and WT/*ahk3*; (B) WT/WT, WT/*ahk3*, WT/*abcg14*, and WT/*ahk3 abcg14*; (E) WT/WT, WT/*ckx4-1*, and WT/*ckx4-2*. (C) Root expression of *IPT3*, *IPT7*, *CYP735A1*, *CYP735A2, CKX1*, *CKX3*, *CKX4*, *CKX5*, *CKX6*, *CKX7*, *UGT76C1*, *UGT76C2*, and *UGT85A1* 4 hours after transfer. Heatmaps were generated with MORPHEUS (https://software.broadinstitute.org/morpheus) from log_2 fold change values relative to WT/WT under 5 mM NH_4^+ + 0.5 mM KCl (set = 1). Color scale: blue (minimum) to yellow (maximum) per row. (D) RT-PCR analysis of *CKX4* in WT, *ckx4-1*, and *ckx4-2* seedlings grown 7 days on 1/2 MS medium. *TIP41* was the control. Primers are listed in Supplementary Table S8. Data are shown as mean ± SD with replicates as follows: (A) n = 18, two replicates; (B) n = 18, three replicates; (C) n = 6, two replicates; (E) n = 24, four replicates. Asterisks (**P* < 0.05, ***P* < 0.01, ****P* < 0.001) mark significant differences relative to WT/WT under 5 mM NH_4^+ + 0.5 mM KCl (Dunnett's test). Pairwise comparisons used Welch's *t*-tests (A). For multiple treatments vs. one control, we used Dunnett's tests (B, E). Significant differences are shown by asterisks above horizontal lines. Graph numbers indicate mean values relative to WT/WT under 5 mM NH_4^+ + 0.5 mM KCl (set = 1). Grafted plants are denoted as "scion line/rootstock line." WT, Col-0; *a3*, *ahk3-7*; *g14*, *abcg14*; *a3g14*, *ahk3-7 abcg14*; *c4-1*, *ckx4-1*; *c4-2*, *ckx4-2*; ns, not significant; KCl, 5 mM NH_4^+ + 0.5 mM KCl; KNO_3, 5 mM NH_4^+ + 0.5 mM KNO_3.